INVESTIGATING THE EFFECT OF MICRO-DIMPLING SURFACE TEXTURE ON CERAMIC-ON-CERAMIC HIP JOINTS

TAPOSH ROY

DISSERTATION SUBMITTED IN PARTIAL FULFILLMENT OF THE REQUIREMENTS FOR THE DEGREE OF MASTER OF ENGINEERING SCIENCE

DEPARTMENT OF BIOMEDICAL ENGINEERING

FACULTY OF ENGINEERING

UNIVERSITY MALAYA

KUALA LUMPUR

2014

UNIVERSITY MALAYA

ORIGINAL LITERARY WORK DECLARATION

Name of Candidate: Taposh Roy

Registration/Matric No: **KGA120022**

Name of Degree: Master of Engineering Science

Title of Project Paper/ Research Report/ Dissertation/ Thesis ("This Work"):

Investigating the effect of micro-dimpling surface texture on ceramic-on-ceramic hip joints

Field of Study: Biotribology

I do solemnly and sincerely declare that:

(1) I am the sole author/writer of this Work;
(2) This work is original;
(3) Any use of any work in which copyright exists was done by way of fair dealing and for permitted purpose and any excerpt from, or reference to or reproduction of any copyright work has been disclose expressly and sufficiently and the title of the Work and its authorship have been acknowledge in this Work;
(4) I do not have any actual knowledge nor do I ought reasonably to know that the making of this work constitutes an infringement of any copyright work;
(5) I hereby assign all and every rights in the copyright to this work to the University of Malaya (UM), who henceforth shall be owner of the copyright in this work and that any written consent of UM having been first had and obtained;
(6) I am fully aware that if in the course of making this work I have infringed any copyright whether intentionally or otherwise, I am be subject to legal action or any other action as may be determined by UM.

Candidate's Signature

Date

Subscribed and solemnly declared before,

Witness's Signature

Date

Name:
Designation:

ABSTRAK

Alumina (Al_2O_3) merupakan bahan yang mempunyai potensi besar untuk digunakan sebagai i implan bioperubatan, ini disebabkan oleh kadar kehausan yang rendah dan biokompatibel. Teknik lekukkan permukaan yang bersaiz mikro adalah salah satu daripada teknik modifikasi permukaan yang paling maju yang didapati untuk pengoptimuman prestasi tribologi. Permukaan lekuk yang jelas pada substrat Al_2O_3 boleh memperbaiki ciri-ciri tribological implan. Dalam kajian ini, satu mesin gerudi mikro CNC digunakan untuk membuat lekuk mikro yang jelas pada Al_2O_3, dan ujian tribologi dijalankan untuk mengoptimumkan parameter lekuk untuk prestasi tribologi yang lebih baik. Morfologi permukaan, kekerasan mikro dan tegasan permukaan lekuk mikro dikaraktesi dan ia menunjukkan bahawa penggerudian mikro CNC boleh digunakan untuk mereka lekuk mikro yang terkawal dari segi corak dan tatasusunan. Kekuatan mikro yang berhampiran pada lekuk adalah sedikit lebih rendah berbanding dengan kawasan selain daripada pinggir lekuk dan permukaan lekuk pada sisa mampatan. Eksperimen tribologi telah dijalakan dengan menggunakan simulasi pinggul di mana ia menunjukkan m peningkatan yang ketara dari segi pekali geseran dan kadar hausan (dari segi kehilangan berat). Pekali geseran mengurang sebanyak 17% - 23% iaitu 181-257 MPa tekanan sentuhan menghampiri15% daripada permukaan lekuk (Ø400 μm, kedalaman 30 μm, nisbah kawasan: 15%) berbanding dengan permukaan yang tidak lekuk. Kadar kehausan (dari segi kehilangan berat) didapati agak kecil dalam magnitud, dipadankan dengan penurunan dalam saiz debris kehausan. Debris kehausan yang paling besar didapati kira-kira 600-700 nm (diameter bersamaa), saiz yang boleh dimuat ke dalam lekuk, maka kemungkinan mengurangkan kesan haus. Kesimpulannya, penggerudian mikro CNC merupakan satu kaedah yang tepat untuk rekaan mikro lekuk pada permukaan Al_2O_3. Selanjutnya, permukaan mikro lekuk boleh digunakan dalam

sendi pinggul seramik pada seramik untuk pengurangan pekali geseran dan pengeluaran debris kehausan wear debris dari kawasan sentuhan.

ABSTRACT

Alumina (Al_2O_3) is a material with high potential for use in bio-medical implants because of its low wear rate and excellent bio-compatibility. The micro dimpling surface technique is one of the most advanced surface modification techniques available for the optimization of tribological performance. A well-defined dimple surface fabricated on Al_2O_3 substrate could further improve tribological properties of an implant. In this study, a CNC micro drilling machine was used to create a well-defined micro dimple patterns on Al_2O_3, and tribology testing was performed to optimize the dimple parameters for better tribological performance. Surface morphology, micro hardness and residual stress of the fabricated micro dimple surfaces were characterized, demonstrating that CNC micro drilling is capable of efficiently fabricating micro dimples with a controllable dimple size and array pattern. The micro hardness very near to the dimple is a little bit lower with compared to the area apart from the dimple periphery and on the dimpled surface it was found compressive residual stress. Tribology experiment was performed in simulated hip joint conditions which revealed an obvious improvement in terms of the friction coefficient and wear rate (in terms of weight loss). The friction coefficient was reduced by between 17% - 23% at 181-257 MPa contact pressures to the where with 15% of the dimpled surface (Ø400 µm, depth 30 µm, area ratio: 15%) compared to non-dimpled surface. Wear rate (in terms of weight loss) was found to be somewhat smaller in magnitude, matched by a reduction in wear particle size. The largest wear debris was found to be approximately 600-700 nm sized (equivalent diameter), a size which could be certainly stored in the dimple, thus reducing their possible abrasive wear effects. In conclusion, CNC micro drilling provides a method for precise micro fabrication of micro dimple arrays on Al_2O_3 surfaces. Further, a well-defined micro dimple surface can be implemented in ceramic

on ceramic hip joints in order to produce a reduction in friction coefficient and removing wear debris from the contact area.

ACKNOWLEDGEMENT

With the deepest gratitude, I would like to gratefully acknowledge the immense support and assistance provided by my supervisors Dr. Dipankar Chowdhury and Dr. Belinda Murphy. Working with them was always inspiring and provided a great experience in engineering and academic research. The patience and committed enthusiasm of Dr. Dipankar Chowdhury in all stages of this work was remarkably valuable towards achieving the successful outcomes from this research.

I would like to acknowledge and express my gratitude to the Dr. Azuddin who has helped me in my sample preparation with the CNC assisted drilling machine and Dr. Sumit who has assisted me on using the FESEM. Never forgetting to thank my workmate Mehdi Mehrali for giving me suggestion and share some experience with me.

I wish to express my appreciation to everyone who has come into my life and inspired, touched, and illuminated me through their presence. I have learned something from all of you to make my project a valuable as well as an enjoyable one. Thank you.

Finally, I would like to take this opportunity to express my sincere gratitude to my parents, whose encouragement have always been precious.

Table of Contents

List of Figures:

List of Tables:

List of Abbreviations

AJM	Abrasive Jet Machining
CoC	Ceramic-on-Ceramic
Co–Cr–Mo	Cobalt-Chromium-Molybdenum
COF	Coefficient of Friction
CNC	Computer numerical control
DC	Direct current
ECM	Electrochemical Machining
EDM	Electrical discharge machining
EDX	Energy-Dispersive X-Ray Spectroscopy
EHL	Electro Hydrodynamic Lubrication
FESEM	Field Emission Scanning Electron Microscope
LASER	Light Amplification by Stimulated Emission of Radiation

LBM	Laser Beam Machining
LT/LST	Laser Surface Texturing
MoM	Metal-on-Metal
Nd:YAG	Neodymium-Doped Yttrium Aluminum Garnet
PDMS	Polydimethylsiloxane
UHMWPE	Ultra-High-Molecular-Weight Polyethylene
WJM	Water Jet Machining
XRD	X-Ray Diffraction

List of Symbols

2D	Two Dimensional
3D	Three dimensional
A	Area
Al_2O_3	Alumina
°C	Degree Celsius
Co	Cobalt
Cr	Chromium
CO_2	Carbon di oxide
E	elasticity modulus

F	Force
fs	Fetom second
g	gram
GPa	Gigapascal
i.e.	That is
kg	Kilogram
L	Length
MPa	Mega Pascal
m	Meter
min	Minute
ml	Mililiter
mm	Millimeter
mm/s	Millimeter per second
Mo	Molybdenum
nm	Nanometer
N	Newton
Pa	Pascal
t	Thickness

T	Temperature
wt%	Weight percent
XRD	X-Ray Diffraction
Y	Geometric factor for residual stresses
σ	Stress
σ_R	Residual stress
μm	Micrometer
ν	Poisson's ratio

Chapter 1.0 Introduction

1.1 Introduction

Hip implants account for the second highest number of procedures (approximately 800,000 in the world per annum). Despite of a success story of hip joints, their application is limited to elderly patients (above 50 years old) because of their limited lifetime. Hip prosthesis manufacturers are trying to increase the survivorship of the hip joint by improving material combinations and design (Ingham et al., 2005). Surgical techniques have also improved, with more accurate and less time-consuming operations. The artificial hip joints may perform well for up to 25 years with good adjustment in the implanted area and under normal walking conditions. However, with young patients having more active lifestyles some implants only last for 10-15 years (Jhurani et al., 2010). Moreover, revision hip replacement is always a more complex and costly surgical procedure (average in Germany - US$18,500) compared to primary hip replacement (average in Germany - US$10,500), partially due to the need to counteract the bone loss, which requires sophisticated anchoring devices fitted to support the prosthesis. Indeed, Life span with active lifestyle is the main challenge for artificial hip prosthesis.

Traditionally, metal on polyethylene and ceramic on polyethylene are the most common types of hip joints prosthesis available to the osteoarthritis patients. However, ceramic-on-ceramic (CoC) prosthesis has become one of the most attractive hip joint prosthesis due to very low friction and wear rate. The brittleness is still a concern of CoC, especially at higher impact load during various active gaits. A Numbers of studies have been carried out in order to minimize the brittleness of Ceramic based hip prosthesis. Most of them are material based including Alumina-Zirconia composite

(Ben Zaïda, 2008; Roualdes et al., 2010). Although most of these finding demonstrated a clear improvement of crack growth resistance, however their long-term results have not been published yet.

Wear of an artificial hip joint is a complex process and is related to a number of parameters including human factors such as body weight; age; level of activity; and implant factors, such as the coefficient of friction (related to fatigue and adhesive wear), surface roughness, material composition, hardness, number of gait cycles and wear debris (Ingham et al., 2005). Thus, an efficient lubrication mechanism could be effective in reducing friction and hence, wear in metal-on-metal hip replacement (Jhurani et al., 2010). Correct lubrication can successfully separate the mating surfaces and promote comfortable movement with the least amount of friction and wear. Synovial fluid is believed to be the best joint lubricant in the body and is found in hip, knee and shoulder joints. However, one major concern for the researcher is how disrupted synovial fluid acts when in contact with artificial surfaces. Furthermore, some synovial fluid is damaged during the hip replacement operation. With this in mind, the quantity and quality of synovial fluid after a surgical operation are not the same as would be expected from healthy synovial fluid. However, these post-operational synovial fluid is only lubricant available in the replaced hip joints and by modifying surface property these synovial fluid can be utilized effectively.

The benefit of surface textures has been well established in engineering surface interfaces, and it application also is tested in hip joints interfaces. For example, Gao et al. (Gao et al., 2010) conducted a theoretical studies of micro-dimpled surface on metal-on-metal hip joints and recommended its high potentiality. Few authors have applied surface texture techniques to joint bearing surfaces experimentally (Choudhury, Walker, Shirvani, et al., 2013; Roy et al., 2014; Sawano et al., 2009a). For example, Sawano et

al. (Sawano et al., 2009a) conducted an investigation aiming to improve wear resistance of metal (Co–Cr–Mo) on polyethylene (UHMWPE) hip joints. After considering a number of assumptions, the result of the study demonstrated that a 1 μm deep dimpled surface was successful at reducing the amount of wear by up to 61% compared with a mirrored surface. However, a 2 μm deep dimpled surface was the worst for reducing wear. Controlling of wear debris and retaining lubrication are behind the success story of the dimpled surface. Ito et al. (Ito et al., 2000) conducted a much more realistic tribological test to identify the effect of a dimpled surface on metal (Co–Cr) on polyethylene (UHMWPE) hip joints on the hip simulator that represented the load and motion of hip joints. A significant percentage of friction (30%) and wear rate (68%) was reduced after 10^6 cycles with a well-designed dimpled surface (Ø 0.5 mm, pitch of 1.2 mm, and depth of 0.1 mm). However, Distilled water was used as a lubricant rather than synovial fluid or bovine serum and the applied load was static (200 kgf load). Choudhury et al. (Choudhury, Walker, Roy, et al., 2013; Choudhury, Walker, Shirvani, et al., 2013) conducted both theoretical and experimental investigations on simulated metal on metal hip joints, and came in conclusion that a well-defined honed surface (width 40±5 μm, depth 17±1.5 μm and spacing 375 μm) is very potential in the hip joint interface since it was found to increase hydrodynamic pressure, capture wear debris and lower friction coefficient. Roy et al. (Roy et al., 2014) also revealed that a significant friction coefficient can be reduced by using micro dimple surface (diameter 400 μm, depth 20 μm and spacing 1 mm) in simulated ceramic on ceramic hip joints. However, an investigation conducted by Zhou et al. (X. Zhou et al., 2012) reported an increased wear rate with the dimple surfaces (diameter 1 mm, depth 1-6 micron and spacing 4 mm) which were rubbed against polyethylene pin. Most of these above studies, textured surfaces (mainly dimpled surfaces) were found to be superior in lubricant distribution, hydrodynamic pressure generation, removing wear debris and result in increasing load

carrying capacity and decreasing wear and friction. However, no study has been conducted on fabrication of micro dimpled surfaces on CoC hip joints.

1.2 Scope of surface texture technique in artificial hip joint surfaces

An optimized geometry of a dimple surface in a particular interface is an attractive research topic among the tribologist around the globe. Our main goal of the study was to understand better the tribological enhancement mechanisms attributed to the dimpled surface of artificial CoC hip joint.

The surface texture, such as micro-dimples or grooves, has been a well-known approach to improve tribological performances of sliding surfaces. Reserving lubricant to prevent seizure should be the earliest understanding of the lubricating mechanism of surface texture. Surface texture technique performs in a superior way in bearing surfaces due to it decreasing the surface contact area, which would have the effect of reducing the coefficient of friction, and trapping wear debris would also prevent severe wear on the surface. This would also have the effect of producing higher hydrodynamic fluid film thickness by acting as a reservoir to provide a good distribution of lubricant to the contact surface. A significant friction and wear rate reduction were reported in MoM and MoP hip joint prosthesis. Our study is the first study that focuses on the fabrication of a micro dimple based on the hypothesis as follows:

Hypothesis 1 – Micro-dimple textured surface would decrease friction and wear rate of ceramic-on-ceramic hip prosthesis.

Hypothesis 2 – Geometry of dimple (diameters, area ration and depth) have an influence on the tribological performances of CoC hip joints.

1.3 Research questions

The research questions of the thesis are-

- How do the tribology properties of dimpled surface improve in ceramic-on-ceramic hip prosthesis compare with those of non-dimpled surfaces?
- How do micro-dimple parameters of textured surface affect the tribological performance of ceramic-on-ceramic hip joint surfaces?

1.4 Aim of the Study

This research has been carried out to investigate the scope and effect of a micro-dimple texture surface technique in low-speed ceramic-on-ceramic hip joints, which could provide lower friction and wear rate, thus enhancing the durability and improving the acceptability of ceramic-on-ceramic hip joints. In order to achieve this goal, different surface profiles were investigated (dimpled and non-dimpled) using bovine serum. By comparing friction coefficients, weight lost rate, surface condition after test and the morphology of wear debris, the best surface profile was selected for CoC prosthesis. This will contribute to the long-term longevity of the prosthesis. The wear debris will also be collected and measured their shapes in order to predict their 'third-body abrasive' wear mechanisms. There are a relatively large number of parameters that are involved in defining a dimpled surface such as the shape, type, number and the arrangement of dimpled on the bearing surface as well as other geometrical parameters such as their height (or depth), pitch and size. In addition, the working conditions such as contact pressure between two bearing joint surfaces, lubricant, sliding speed can influence the performance of the artificial bearings. Considering these issues, an experimental research was conducted to improved tribological outcomes of dimple surface. The current research objectives can be subdivided as follows:

i. To produce well define dimple surface texture on ceramic.

ii. To characterize the dimpled surfaces.

iii. To investigate the mechanical properties of dimpled surfaces.

iv. To investigate the tribological performances of micro-dimpled surface on simulated ceramic-on-ceramic hip joints.

Chapter 2.0 Literature review

2.1 Background

From the last century, it has been observed that the modification of surface properties, predominantly at micro and nonometer scale, has played a fundamental role in the development of several advance fields, especially on tribology, biotribology, biomimetics, biology, energy, optics, electronics, information technology, etc. Also researcher established several technic with a vast technologies in the area of micro fabrication. Several function of surface phenomenon has been exploited as many established technic are available to create surface feature with sizes in micro and nanometer ranges. Although the manufacturing of surface feature on nanometer range is still challenging, and has also been the subject of intensive research and development.

2.2 Surface texturing Technologies:

Researchers has developed the surface modification technic both conventional and nonconventional manufacturing processes over the year. In this sections it has been discussed the modification of surface topography relating with the manufacturing technic that improve or exploit the surface properties, mainly considered the micro texturing. Also reviewed the attributes, advantages, disadvantages and application, through literature survey as the precision surface texturing is the subject of extensive studies, focusing both on new texturing methods and on applications of textured surfaces. Figure 2.1 shows the general methods for removing material of the surface for creating surface texturing.

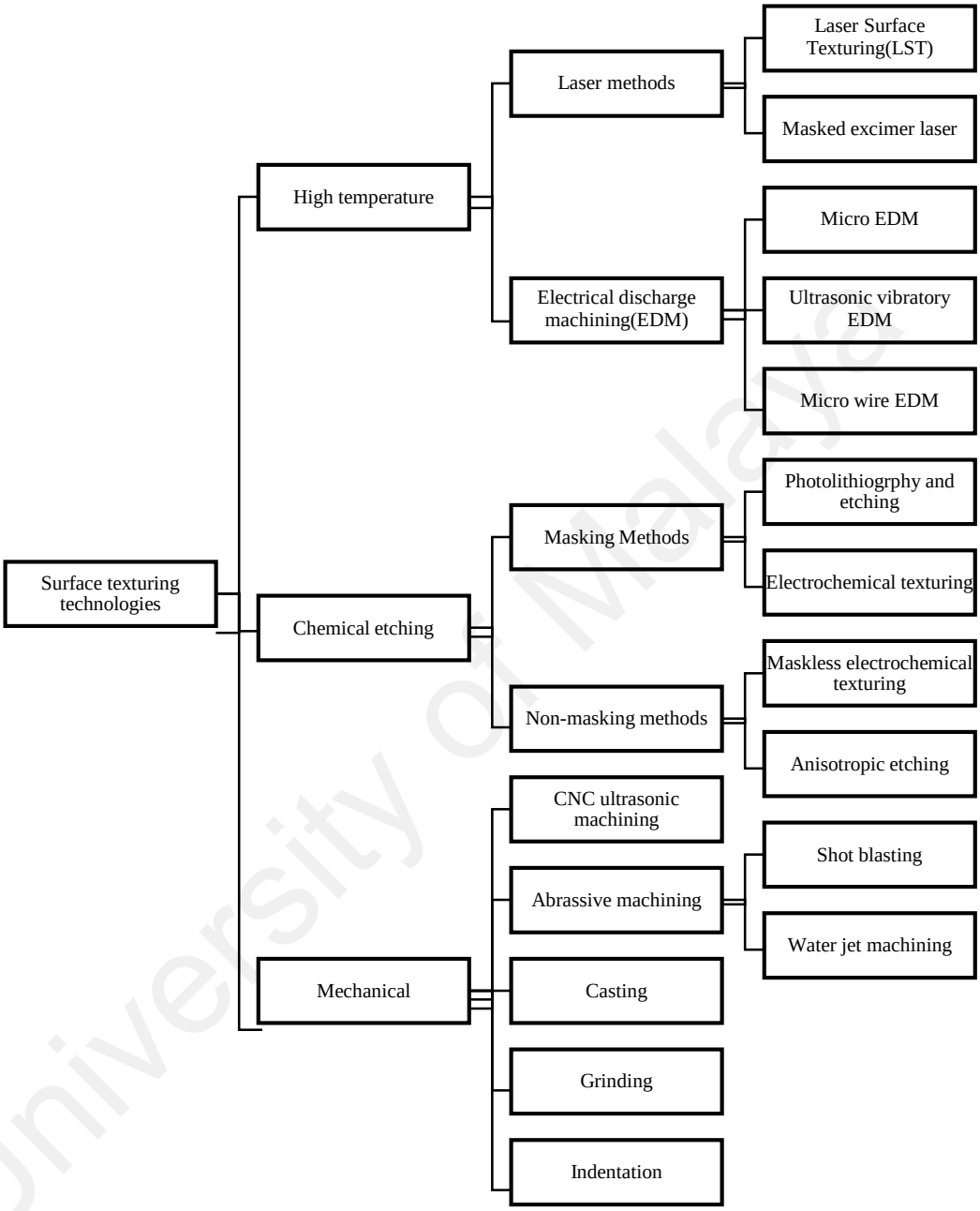

Figure 2.1:General micro fabrication surface texturing technologies

2.2.1 Laser Surface Texturing (LST):

Laser surface texturing is a non-contact machining process. High density optical energy originated from laser (Light Amplification by Stimulated Emission of Radiation) is the main source of energy which is used on the surface of the work piece and the material is removed by melting, dissociation, and evaporation and material expulsion from the area of laser–material interaction. More than 40 years of the development of the laser, laser surface texturing performed very precise manufacturing almost every matting surface, and also there is a lot of effort in developing new and better performing lasers.

Table 2.1 shows the different type of short pulsed laser.

Laser	Wavelength (nm)	Pulse length	Frequency (kHz)
CO_2	10600	200 µs	5
Nd:YAG	1060, 532, 355, 266	100 ns 10 ns	50
Excimer	193–351	20 ns	0.1-1
Copper vapor	611–578	30 ns	4–20
Ti Sapphire	775	100 fs	1-250

Table 2.1: Different type short laser (Johan Meijer, 2004)

Laser	Wavelength (nm)	Pulse length	Frequency (kHz)
CO_2	10600	200 µs	5
Nd:YAG	1060, 532, 355, 266	100 ns 10 ns	50
Excimer	193–351	20 ns	0.1-1
Copper vapor	611–578	30 ns	4–20
Ti Sapphire	775	100 fs	1-250

Among different type of lasers, Nd:YAG and CO_2 are most widely used for LBM application. CO_2 lasers have wavelength of 10 μm in infrared region. It has high average beam power, better efficiency and good beam quality. The primary difference between a Nd:YAG and a CO_2 laser, for purposes of engraving and part marking, is the wavelength of the laser beam. The light of a Nd:YAG laser is emitted at a wavelength of 1.064 microns - precisely 10 times smaller than that of a CO_2. Nd:YAG lasers have low beam power but when operating in pulsed mode high peak powers enable it to machine even thicker materials. Also, shorter pulse duration suits for machining of thinner materials. Due to shorter wavelength (1 μm) it can be absorbed by high reflective materials which are difficult to machine by CO_2 lasers (Dubey et al., 2008).

For precise manufacturing now a days it has been developed ultra-short laser. The incident photon from laser, absorb the free electron of the skin layer of substrate. The absorbing time is about 1fs and the optical penetration depth is 10nm. The relaxation time of the electron is about 1ps. In this time the energy stored in the electron layer about 10nm and then converted into heat. The heat is diffused from skin layer to substrate. For steel it takes 1ps for thermal diffusion at the depth 10nm. Thus it is called ultra-short laser, if the thermal diffusion depth is equal or shorter than the skin layer penetration depth (J Meijer et al., 2002). It is considered to be ultra-short laser if its time is shorter than 1ps, 10ps and 1ns for steel, ceramic and plastic, respectively (Johan Meijer, 2004). The advantages of ultra-short laser, heat does not have enough time to diffuse into the material depth. So it does not create the heat affected zone. Therefore nearly no surface debris, recast layer in the machining zone, adjacent layer of the substrate does not affected. Which improve the tribological effect. The comparison between “long” and “ultra-short” laser are shown in Figure 2.2.

In micro fabrication Q. Switch Nd:YAG is better because of it lower wave length of the laser. Most of the researcher in tribology who has done micro fabrication by laser, they used Q. Switched Nd:YAG (Andersson et al., 2007; Hu et al., 2012; Podgornik et al., 2012; Sampedro et al., 2012; Vilhena et al., 2009; Yamakiri et al., 2011). They has used one wave length 1064nm. For getting different size and pattern, changed the power of the peak laser. Because use of the short laser pulse, bulges or burrs has been created, which need to further polishing. And the precision was not that much controlled with compare to ultra-short laser pulse, Sampedro et al. (Sampedro et al., 2012) used third harmonic ultra-short laser pulse 10ps with wave length 343nm. The fabrication was very precise and negligible bulges formed. In micro fabrication, shorter pulses reduced the bulges formation, precise manufacturing, reduce the heat affected zone (Andersson et al., 2007; Borghi et al., 2008; Kovalchenko et al., 2011)

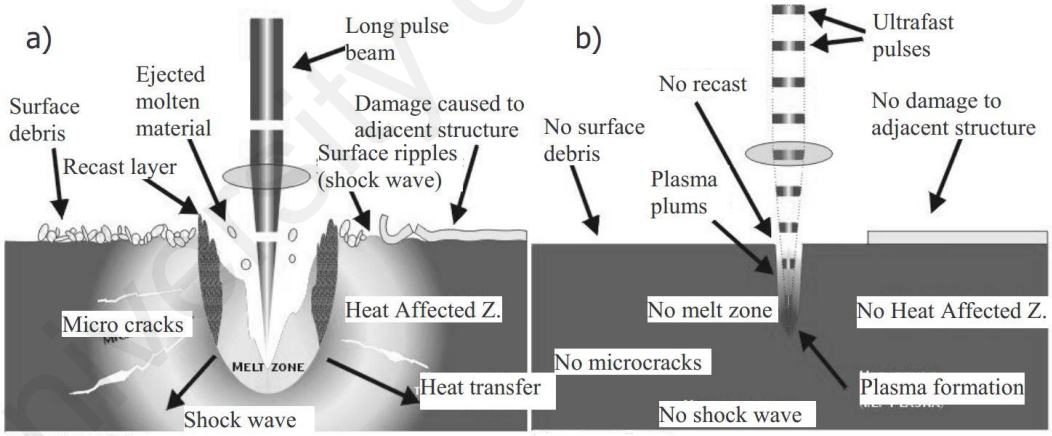

Figure 2.2: Comparison of laser machining quality, a) by long pulse laser (15ns), by ultra-short pulse laser (150fs) (PAJAK et al., 2005)

2.2.2 Electrical Discharge Machining (EDM):

Electrical Discharge Machining (EDM) is a non-contact, no-conventional machining process which can be applied only on the fabrication of electrically conductive material. It is a well-established machining process option regardless the material hardness and complexity of the geometry that are very difficult to fabricate by the conventional machining process. Thermoelectric energy, produced by precisely controlled sparks that occur between the tool and workpiece in the presence of a dielectric fluid (Jameson, 2001) is used in the EDM machining process. EDM is based on the melting and vaporization of tool and workpiece material during the high frequency spark time (Llanes et al., 2001). Thus, EDM is based on the no-contact erosion process between the tool and workpiece that can eliminate the mechanical stresses, chatter and vibration problem during machining process (Ho et al., 2003; Mohd Abbas et al., 2007).

After the establishment of EDM process in the late 1940s (S. Singh et al., 2004), it has been influenced a great development in the micro fabrication with various new method such as ultrasonic vibration EDM and wire EDM. Many researchers (Huang et al., 2003; Shin et al., 2011; Thoe et al., 1999; Wansheng et al., 2002; B. Yan et al., 2002; Yeo et al., 1999) have been studied on ultrasonic vibration EDM after the first development by Zhixin et al. (Zhixin et al., 1995). EDM is capable to fabricate holes and shaft as small as 3μm in diameter but also can produce very complex three dimensional (3D) micro cavities (T Masuzawa et al., 1994; Takahisa Masuzawa, 2000; Rajurkar et al., 2000; Z. Yu et al., 1998; R. Zhou et al., 2011). Wire EDM is preferable to fabricate precise microgrooves in surface texturing (Fleischer et al., 2004; Ho et al., 2004; Puri et al., 2003; Rajurkar et al., 1993)

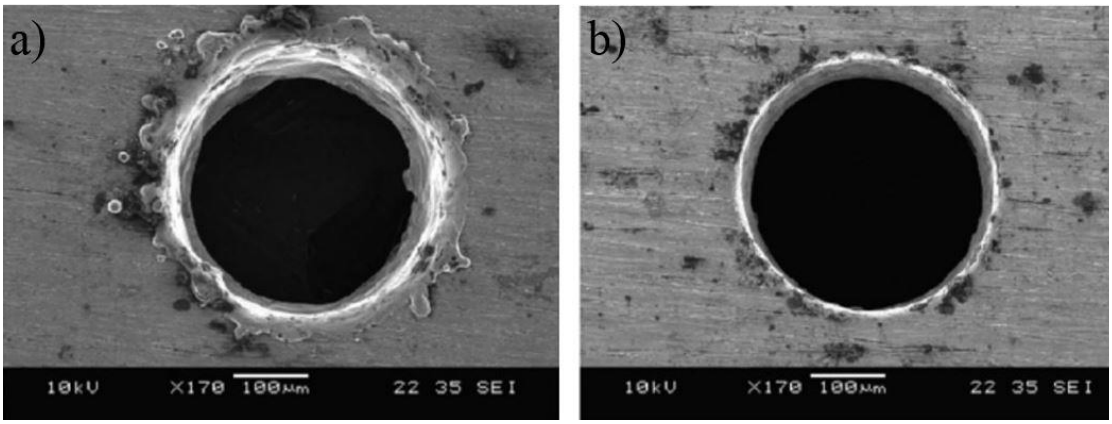

Figure 2.3: Comparison of micro-hole fabricated on tungsten carbide by, a) RC-type pulse generator (at 140V, 6.8Ω, 960.78J); b) transistor type pulse generator (at 80V, 100Ω, 21.33J) using 300µm tungsten electrodes with EDM machining process (Jahan et al., 2009)

Several numerical simulation and experimental study (Dhanik & Joshi, 2005; Katz et al., 2005) showed that the precise manufacturing process depends on the current density, crater area, power dissipation and the rate of channel growth. Jahan et al. (Jahan et al., 2009) showed that RC-type pulse generator fabricate good surface quality with rim free of burr-like recast layer, very good precise in dimension than transistor type pulse generator. Figure 2.3 shows the comparison of surface quality of micro-hole produced on tungsten carbide by RC-type pulse generator and transistor type pulse generator. Dhanik et al. (Dhanik, Joshi, et al., 2005), Jahan et al. (Jahan et al., 2011) provide review of EDM modelling to predict the output parameters of EDM process and propose the future development of precise manufacturing.

2.2.3 Chemical Etching:

Electrochemical machining (ECM) is another non-traditional, non-contact chemical etching material removal technology governed by Faraday's laws of electrolysis(Rajurkar et al., 2013) includes cathodic, anodic and open circuit processes, which generates closely mirror image of the tool on the substrate(Rajurkar, Zhu, et al., 1999). The ECM process was first introduced by Gusseff in 1929 and thereafter in 1950s and 1960s it advanced in to the major technologies in the aerospace (Huaiqian et al., 2008; Pavlinich et al., 2008), biomedical (Dhobe et al., 2011; Kamaraj et al., 2013), deburring (Kilickap et al., 2010), tribology (Parreira et al., 2012) for shaping, finishing, milling operation of the large parts (Rajurkar et al., 2013). The advantages of this process is no tool wear, absence of stress or burr, high metal removal rate, bright surface finish and able to fabricate very complex shape regardless of the hardness of the material. In the miniaturization of various ultraprecision fabrication technologies for fabricating highly precise machine equipment and accessories, ECM deals with the micro fabrication ranges with micro-millimetre is called micro electrochemical machining (EMM)(Bhattacharyya et al., 2002). ECM process depends on the electrochemical properties of the metal, properties of electrolyte and supplied electrical voltage/current.

ECM process can be divided as masking method and non-masking method. In masking method photolithography can be mentioned, where a chemical reagent is applied to the surface to remove material from the specific area. Thus almost any complex irregular shape can be fabricated. Shu et al.(Takami et al., 1997) fabricated micro texture on steel. They generated micro grooves, 40µm-100µm with different angle by photolithography technique us. In etching process they used NaCl electrolyte with 4 V and 542 mA. The texturing was highly precise. In very hard material of diamond like carbon (DLC), Chouquet et al.(Chouquet et al., 2010) used

photolithography for surface texturing. They successfully fabricated very precise micro hole of 7µm and 65µm with very small depth of 1.3µm.Photolithography technique also used to fabricate micro hole and micro groove by Yan et al.(D. Yan et al., 2010), Yuan et al.(Yuan et al., 2011), Wang et al.(X. Wang et al., 2009). Half circle micro hole was produced by Lu and Khonsari(Lu et al., 2007). Costa and Hutchings (Costa et al., 2007) also produced other possible different pattern using photolithography.

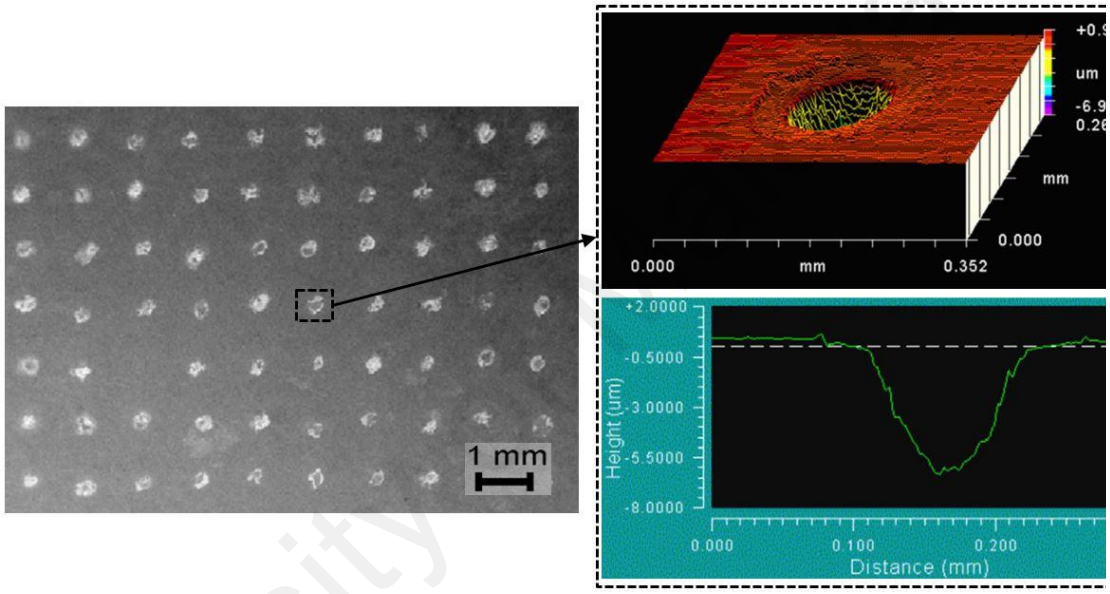

Figure 2.4: SEM of a surface texture obtained with MECT and Profile of an individual pocket obtained with Maskless ECM (Costa, 2005; Costa et al., 2009)

Although ECM does not produce mechanical or thermal damage, burrs, and debris, for getting precise manufacturing, good surface quality Byun et al.(Byun et al., 2010) uses short pulses of a microsecond pulse on-time and found better result. For reducing the fabrication process and cost, Zhu et al.(Zhu et al., 2009) proposed a new method through mask ECM(Findlay et al., 2004). They re-used the mask again and again for reducing time. Maskless ECM is comparatively cheap and simple as no printing needed

(Byun et al., 2010). Costa (Costa, 2005; Costa et al., 2009) proposed and implemented other possible masking the maskless electrochemical machining. Figure 2.4 shows example of a texture obtained using the optimized conditions and the profile of an individual pocket as imaged by optical interferometry.

2.2.4 Mechanical Machining:

The miniaturization of fabrication of micro pattern and micro work piece has been essentially the same since manufacturing was first established as an art/science – new applications, better performance, less expensive and higher quality. Both conventional and non-conventional machining process has played a great role in the development in precise manufacturing. Taniguchi (Taniguchi, 1983), Byrne et al. (Byrne et al., 2003) reviewed the possible micro machining in the ensuing two decades. In the conventional mechanical machining process, it can be mentioned indentation, milling, grinding, ultrasonic machining, drilling etc. In non-conventional process, it can be mentioned shot blasting, water jet machining, abrasive water jet machining etc. Micro casting is another fabrication process which can be used as a precise micro manufacturing. Nakano et al. (Nakano et al., 2007) used the micro milling and shot blasting. In shot blasting, hard shot particles impact the surface at high velocity to cause impact damage and roughening of the surface. The change in the surface structure is attributable to plastic deformation. It is difficult to precisely control the texture because of the large number of variables inherent in the process, such as the size, shape, velocity and hardness of the shot. Also, shot blasting can only form random textures. Nakano et al (Nakano et al., 2007) used micro milling for creating larger surface texturing and shot blasting to get comparatively small surface texturing and good surface quality. In shot blasting the abrasive particle could be used form removing material from the selective area of the work piece, if the surface is masked with an erosion resistant material. By applying mask shot blasting can get better precise in fabrication and no damage of the

surrounding surface. Wakuda et al. (Wakuda et al., 2003) used water jet machining with using mask and successfully fabricate very precise micro hole of diameter 40, 80 and 120 µm with no burr formation. Indentation is one of the cheapest and simple technique to fabricate pattern on the work piece material (Křupka et al., 2007; Krupka et al., 2010; I. Křupka et al., 2008; Ivan Křupka et al., 2008) by it can't be used on brittle material because of chances to create crack to the surrounding surface. Ultrasonic machining is a very economical, simple and effective method in fabricating pattern of machine components and machinery of various purposes. Ultrasonic energy of high frequency of about 22 kHz and very low and low amplitudes between 4 - 15 µm, is used in ultrasonic machining process. It can be also used for machining brittle ceramic material (Rajurkar, Wang, et al., 1999; R. Singh et al., 2006). Amanov et al. (A Amanov et al., 2012; Auezhan Amanov et al., 2011) fabricate spherical micro dimple with diameter 1.25 µm using modified ultrasonic machining on steel surface. Another economical fabrication process can be stated as micro drilling (Cho et al., 2011; Ma et al., 2011). With the assistance of CNC programming highly precise fabrication can be achieved although there is a limitation with the size of the tool. Several researchers (Dowson et al., 2000; Wei Huang et al., 2012; Ramesh et al., 2012) also used micro casting for fabricating micro dimple

2.2.5 Remarks:

Challenges occur when manufacturing a well-defined surface; the tolerance of the dimensions is precisely maintained at the micro or nano-level. Several manufacturing techniques are well-established and are capable of precisely manufacturing a surface texture at the micro level. It can provide both micro and nano-level surface finishes and precise dimples or grooves. The benefits of chemical etching over other techniques are clear it does not affect the material either in terms of thermal or mechanical properties. Chemical etching is another manufacturing process that uses a controlled light to

create a geometric pattern such as dimple or groove using photolithography, from a photo mask to a light-sensitive substrate. Photolithography techniques are highly effective in producing well-defined geometrical patterns on target surfaces (Illgen II et al., 2009; Love et al., 2012; H. Yu et al., 2010). Chemical etching is effective techniques, but slow.

Various methods has been proposed for improving machining productivity. As number of tool electrodes increased, machining area increased which reduces the machining time (B. Park et al., 2006; M. S. Park et al., 2007). Using different individual pulses generator simultaneously with electrodes, multiple holes with different size can be fabricated (M. S. Park et al., 2007). During machining on ECM, the dissolution rate decreased as the depth of the hole increase because of the electrolyte diffusion and bubble problem. Yang et al. proposed micro ECM with ultrasonic vibrations and experimentally showed, dissolution rate improved with the using ultrasonic vibrations (Yang et al., 2009). For getting better surface quality Jeon et al.(Jeon et al., 2006) used ECM and EDM together and got better surface quality. Materials that exhibit a high degree of brittleness, or hardness, and have favourable thermal properties, such as low thermal diffusivity and conductivity, are particularly well suited for laser machining. This method is typically a mask-free technique, but is costly and requires further lapping and/or polishing prior to application. AJM can fabricate micro texture in difficult-to-reach areas, generating less heat compared with conventional machining processes. Wakuda et al. (Wakuda et al., 2003) fabricated micro dimple on ceramic surface by LST and AJM, Figure 2.5 shows micro dimple fabricated by LST and AJM. CNC micro drilling is another technique used to create precise dimples in metal or ceramic surfaces (Balla et al., 2010).

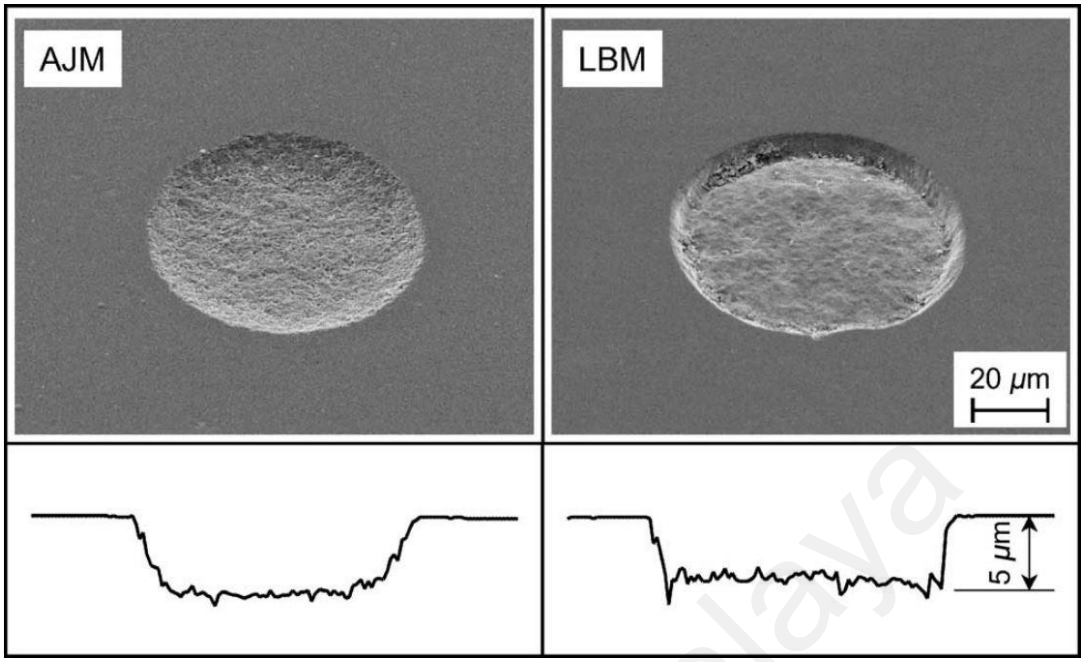

Figure 2.5: SEM image of produced dimple by AJM and LST (Wakuda et al., 2003)

It is an economical manufacturing process, and tolerances can be maintained to very high standards with CNC programming. However, the usefulness of the process depends upon the availability of the specific size and shape of the drill bit. Creating a micro hole less than 200 μm is difficult, particularly when it must drill into hard materials, such as ceramic or chromium cobalt alloys. Ultrasonic machining is a unique manufacturing process (Rajurkar, Wang, et al., 1999; R. Singh et al., 2006; Spur et al., 1996; Tawakoli et al., 2009; C. J. Wang et al., 1994; Yanyan et al., 2009) that can produce micro-textured surfaces at very low cost and faster speed. The initial equipment setup cost for ultrasonic machining is approximately 90% less than that of a comparable laser-based texturing system. Ultrasonic machining can create dimples or grooves with flexible dimensions at a micro or nano-level regardless with the hardness of the work piece material (A Amanov et al., 2012; Auezhan Amanov et al., 2011).

2.3 Influence of surface texture on wear, friction, and lubrication

Plateau honing and dimpling are the two key methods for modifying surface texture that help achieve improved tribological outcomes, including lowering friction and wear, enhancing lubrication pressure and distribution, increasing load-carrying capabilities, and reducing third body abrasive wear (Bruzzone et al., 2008). These methods have been investigated to optimize honed parameters at a micro level since the last century. A dimpled surface is a relatively new technique, but few studies have proved that its potentiality is higher than other methods (Balla et al., 2010). However, in both cases, the optimized parameters were found to be dependent upon experimental conditions, such as load, speed, lubrication, and material.

Wakuda et al. (Wakuda et al., 2003) conducted an experimental study to identify the effect of different geometrically dimensioned dimples (D: 40, 80, or 120 μm, and p: of 7.5%, 15%, and 30%). The test was performed on a unique pin (hardened steel)-on-disk (silicon nitride ceramic) tester with 5W30SJ Engine oil. According to their study (Wakuda et al., 2003), the lowest friction coefficient was produced with a dimpled surface of 120 μm (D) and 15% area density. The output COF was 37% lower compared with that in a non-textured surface at 1.2 m/s sliding speed and 100 N applied load.

For example, a 40 μm dimpled surface (ratio 0.92) showed a COF 0.10 at 0.8 m/s, 490 N, 15% dimple density, whereas the friction coefficient was found to be 0.07 with a dimpled surface of 120 μm diameter (ratio 2.2). Similar to the previous work, Uehara et al. (Uehara et al., 2004) investigated the tribological performance of dimpled surfaces (D: 40, 80, 120 μm; and p: 7.5%, 15%, 30%) under lubricated conditions in hardened bearing steel. Through the experiments, they showed that dimpled surface on the sliding interface could yield both positive and negative effects, depending on the dimple size and density as well as the frictional conditions. Under test conditions, dimpled surface

(D: 40 µm, p: 15%) was the most effective dimpling pattern for reducing friction. However, the performance of the dimpled surface was found to vary with applied loads and sliding speeds. Huang et al. (W. Huang et al., 2012) used dimple parameters of D: 50, 100, 200 µm; H: 5 µm; p: 2.6% to 40.1% that were essentially similar to those used by Wakuda et al. (Wakuda et al., 2003), but produced an opposite friction coefficient. The textured surface with dimples of a higher diameter (200 µm) increased the COF to as high as 1.2 and 1.0 at sliding velocities of 0.003 and 0.006 m/s, respectively, which were 1.4 and 4.0 times higher than that of the un-textured surface, respectively. However, the pattern with smaller dimples (D: 50 µm) decreased the friction coefficient by 69% and 50% of that of the un-textured surface, at similar ranges of sliding speed, respectively. Their material was a softer elastomer, Polydimethylsiloxane (PDMS), in a flat block; a solution of de-ionized water and glycerol was used as a lubricant. Li et al. (Li et al., 2011) also investigated the friction between a steel ball and a PDMS disk under water lubrication and found the same result: at lower speeds, the COF was much higher from dimpled surfaces than in non-dimpled surfaces. Therefore, a harder material is desirable to benefit from the textured surface. Hu et al. (Hu et al., 2012) used a circular dimpled surface (D: 150 µm, H: 40 µm; p: 13%, 23%, and 44%) on a flat alloy block with a Ti-6Al-4 surface with MoS_2 powder used as a solid lubricant. The textured surface (p: 44%) was found to be most effective in leading to a lower and stable COF (0.1 to 0.25), especially under a high load. Interestingly, the non-textured surface was found to lead to an abnormal COF only after 0.25 km to 0.5 km of sliding distance. This abnormality could be attributed to the effective capture of wear debris for the surface with high dimple density. Qian et al. (Qian et al., 2010) assessed the COF of the surface with a micro-dimple array (D: 240, 280 µm, H: 4, 10 µm, p: 14%, 18%).

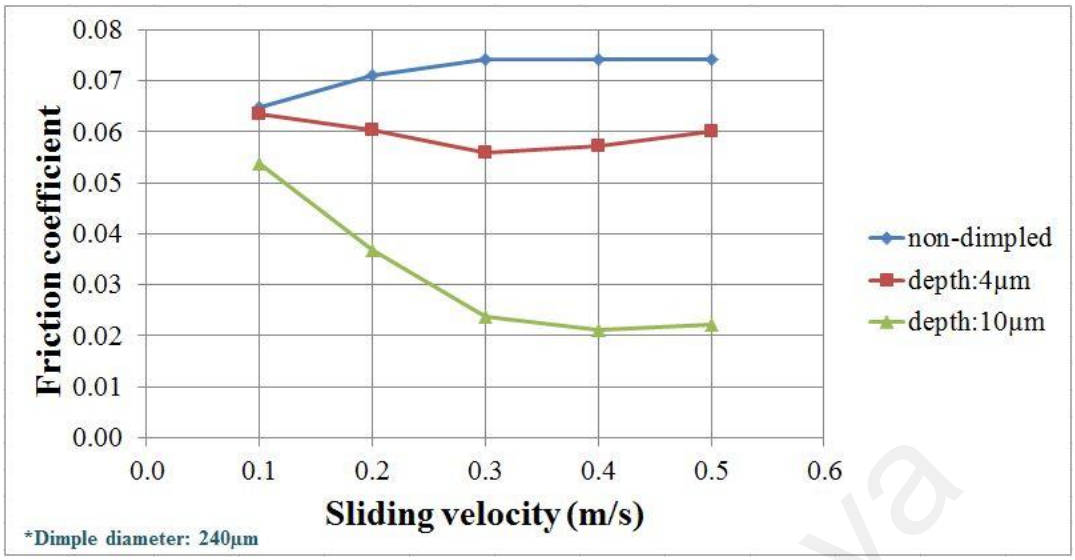

Figure 2.6: Effect of dimple array under applied load of 500 (Qian et al., 2010)

In Figure 2.6, a dimple array with diameter of 240 μm and depth of 10 μm was most successful in lowering COF by 71%, compared with a non-textured surface at a sliding speed of 0.4 m/s and normal load of 500 N.

Kovalchenko et al. (Kovalchenko et al., 2011; Kovalchenko et al., 2005) conducted a series of experiments on dimpled surfaces. In their first work in 2005 (Kovalchenko et al., 2005), they investigated the impact of LST on lubricating regime transitions by using a pin-on-disc apparatus. Six different types of surface with two different types of lubricant at different sliding velocities were tested: un-textured polished, un-textured ground, standard LST with and without lapping, LST with high and low dimple densities. Results showed that at a lower speed (0.0375 m/s), the resultant COF was low with a standard LST, but at higher speed (0.6 m/s), COFs were mostly same for all specimens. In their next paper, in 2011, Kovalchenko et al. (Kovalchenko et al., 2011) investigated the influence of a dimpled surface (D: 58, p: 15%; D: 78, p: 12%) on both

friction and wear. Their results showed that a textured surface is a very effective means of reducing friction. Ramesh et al. (Ramesh et al., 2012) also worked on stainless steel textured by LST with dimple size of 28 μm to 257 μm; they showed that the textured surface reduced 80% in friction coefficient compared with a non-textured surface. However, wear rate was much higher under high pressure due to a decrease in lubricant fluid film thickness. Therefore, the study recommended that a textured surface could be effective in reducing friction through lubrication regime change. However, accelerated wear could make a textured surface tribologically detrimental, where wear is undesirable, especially in those components where high precision and stability of dimension are required. A series of experiments was conducted by Krupka et al. (2007) (Křupka et al., 2007), (2008) (I. Křupka et al., 2008), (2009) (Křupka et al., 2009), (2010) (Krupka et al., 2010). They showed the effect of size and shape of micro-features, as well as of slide-to-roll ratio on lubricant film thickness. Krupka et al. (2010) (Krupka et al., 2010) investigated the effect of a dimpled surface (D: 120 μm, L: 50 μm, H: 0.2 μm) and concluded that a properly defined texture of a bearing surface could reduce the interaction of asperities both during start-up conditions and under transient operational conditions. For example, they showed evidence of increasing 260% and 100% in fluid film thickness compared with a polished surface during start-up and dynamic conditions, respectively.

Qiu et al. (Qiu et al., 2011) used two types of dimple shape with three arrangements, 1) circular, 2) elliptically shaped radially oriented, and 3) elliptically shaped circumferentially oriented, in a tribology test with stainless steel (hardness of 30 HRC and roughness of 0.1 μm) and a lubrication grade of SAE 30. A circumferentially oriented elliptical dimple array with a density of 40% performed best; the entire specimen showed a COF of nearly 0.6 at 800 rpm with a load of 4.5 N, and

0.25 at 800 rpm with load of 18 N. Thus, the dimple size affects load-carrying capacity. Lu et al. (Lu et al., 2007) studied similar patterns of dimpled surfaces (circular, elliptical, and non-textured) on journal bearings and suggested that an elliptical shape could reduce the COF most effectively among their experimental surfaces, particularly at the speed of 1 rpm to 10 rpm. Suh et al. (Suh et al., 2010) used a flat surface with crosshatching on steel (SKD11, JIS), in paraffin oil. Contact pressure was 0.5 MPa to 3.5 MPa and sliding velocity was 0.02 m/s to 0.30 m/s, showing the influence of angle in reducing friction. A similar type of experiment was conducted by Nakano et al. (Nakano et al., 2007), Costa and Hutchings (H. Yu et al., 2010), and Chouquet et al. (Chouquet et al., 2010). Nakano et al. (Nakano et al., 2007) investigated cast iron (ASTM Class No.35). They performed a friction test on three types of texture, using groove, mesh, dimple, and flat polishing and grinding. Dimple pattern was effective in reducing the friction coefficient and load-carrying capacity of the lubricant film. At a normal load of 300 N and speed 0.083 m/s to 1.0 m/s, the most effective pattern was a dimpled pattern (0.01 to 0.02), which reduced friction by 80%–90%. Costa and Hutchings (Costa et al., 2007) worked steel flat plates (AISI 01 GFS) using three types of patterns of circular dimples, grooves, and chevrons with different dimensions, with mineral oil as lubricant. Circular dimples of an area coverage fraction exceeding 0.11 was achieved with a maximum film thickness of 14.2 μm to 4 μm at 10 N to 80 N. They showed that grooves and chevrons pointing along the sliding direction were the most effective as they generated a higher film thickness (15.8 μm to 5 μm) than those pointing across, with an area contact ratio 0.07, a depth-to-width ratio of 0.12, and load of 10 N to 80 N.

A series of experimental works was reported by Wang et al. (2001) (X. Wang et al., 2001), (2003) (X. Wang et al., 2003), (2006) (X. Wang et al., 2006) and (2009) (X.

Wang et al., 2009) on the application of surface-texturing technology by using micro dimples on a SiC surface, working with water as lubricant. In 2003, Wang et al. (X. Wang et al., 2003) investigated the critical load of the textured (micro pit) surface that could transfer the transition of the hydrodynamic lubrication mode to partial mode. The experimental method and materials were almost the same as those in their previous study discussed above, and the shape of pores was cylindrical. Their analyses concluded that the load-carrying capacity could be increased by up to 250% by optimizing pit geometry parameters, such as depth-diameter ratio (1: 110) and area ratio (5%). These optimized parameters contributed in increasing hydrodynamic pressure under the designed experimental conditions, such as load, speed, material, and lubrication.

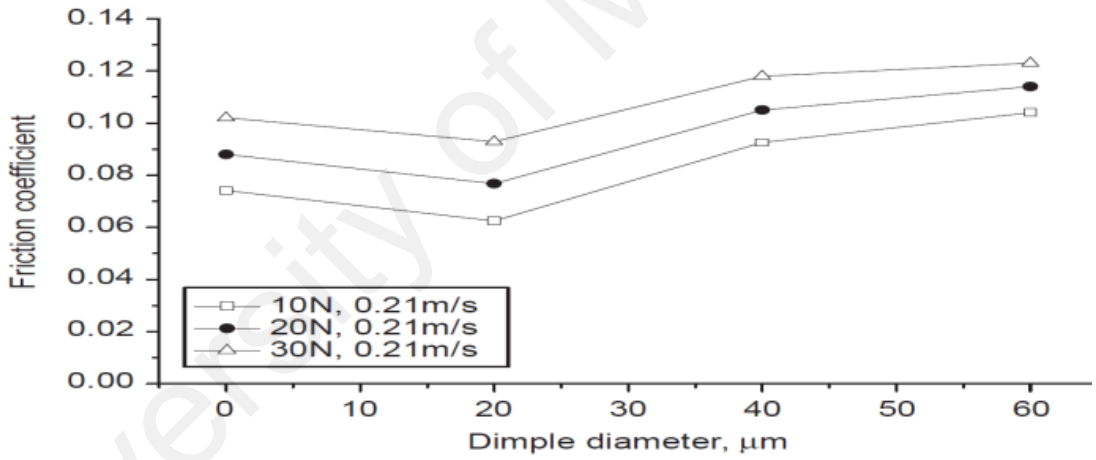

Figure 2.7: Effect of dimple diameter on friction coefficient at 0.21 m/s(X. Wang et al., 2009)

In their next attempt, Wang et al. (2006) (X. Wang et al., 2006) established an optimization of the surface texture for SiC sliding into water to enhance the critical load. They optimized their previous texturing pattern and also investigated other texturing patterns: small square dimples with a side length of 40 mm and a pattern with

a combination of two patterns. They showed the effect of texturing parameters with respect to friction coefficient and the critical load. The critical load for large dimples was greater than that for small ones but overall, both types of textured were improved over the untextured surface. Furthermore, the combined dimples (small and large) performed superior compared with only small or large dimples, increasing the critical load three times that of a smooth surface.

In their last attempt, Wang et al. (X. Wang et al., 2009) investigated the effect of various dimple sizes on friction and load-carrying capacity of an oil-lubricated line contact. In such a case, the methods were both numerical simulation and experimental study. They used dimples with diameters of 20, 40, and 60 μm and depths of 0.6, 1.2, 1.8, respectively, on brass disks with a lubricant of light paraffin oil. The numerical simulation results suggest that the radius of the cylinder and the dimple size are critical factors. In Figure 2.7, dimple diameters of 20 mm at 0.21 m/s presented the best effect on COF, decreasing it by 15.6% at loads of 10 N, by 12.7% at 20 N, and by 8.9% at 30 N.

Several researchers have been working on the application of the surface texturing concept in elasto-hydrodynamic and mixed lubrication. Amongst those researchers, Mourier et al. (Mourier et al., 2006), and Krupka and Hartl (Křupka et al., 2007) are of particular note. Mourier et al. (Mourier et al., 2006) worked on transient lubrication phenomena under pure rolling conditions. Both experimentally and numerically, the study showed that the micro-cavities do not significantly affect the lubricant film thickness. Under rolling-sliding conditions and an EHL regime, deep cavities resulted in a decrease of film thickness or caused fatal collapse of the lubricant layer. On the other hand, shallow micro-cavities significantly improved the lubricant film thickness in a similar environment.

The behavior of an array of micro-dents within thin EHD contacts were studied in an experimental effort by Krupka and Hartl (Křupka et al., 2007). Their goal was to determine whether well-defined micro-dents could alter the thin film thickness in highly loaded non-conformal contact surfaces by varying dent depths. The results within a lubricated zone indicated that the thin film thickness decreased for a set of deep micro-dents, whereas film thickness was thicker for the lighter deep dents. The scenario was not the same in the slide-to-roll conditions; thickness was influenced less in the latter cases.

Costa and Hutchings (Costa et al., 2007) conducted their study using different angles, showing that the film is thicker at slower sliding speeds due to a squeeze-film effect. Importantly, they noticed that the dimpled (diameter>contact width) surface produced thinner film compared with the non-textured surface and vice versa. Moreover, the shape of the dimple influenced performance. For example, the circular dimpled surface achieved a thicker film thickness at the area ratio of 11%. However, no significant effect was observed at low area ratios. Furthermore, the chevron patterns positioned parallel to the sliding direction were found to have thicker films compared with those positioned across the sliding direction. In this case, the area density ratio was 0.06, with a depth-to-width ratio of 0.07. Costa and Hutchings (Costa et al., 2007) also recommended that grooved surfaces with well-defined chevrons are much better in increasing hydrodynamic film thickness compared with only grooved surfaces.

2.4 Scope and challenges of dimpled surface textures for artificial bearing joints

The benefit of surface textures has been well-established in engineering surface interfaces. Few authors have applied surface texture techniques to joint bearing surfaces (Gao et al., 2010; Ito et al., 2000; Sawano et al., 2009a). However, surface texture has

seen a number of applications to a natural skin surface, whose functions are significant in friction reduction and smooth flow. For example, the longitudinal texture on shark skin is found to be efficient in reducing friction (W. Huang et al., 2012). This section summarizes investigations performed with hip or knee joint conditions and their limitations and implications for further study, which will represent a realistic tribological test, shows in Table 2.2.

Four studies were identified as tests in hip joint conditions. One was a numerical analysis; the rest were experimental studies. Sawano et al. (Sawano et al., 2009b) conducted an investigation aiming to improve wear resistance of metal (Co–Cr–Mo) on polyethylene (UHMWPE) hip joints. After considering a number of assumptions, the result of the study demonstrated that a 90 μm deep dimpled surface was successful at reducing the amount of wear by up to 61% compared with a mirrored surface. However, a 2 mm deep dimpled surface was the worst for reducing wear. Sawano et al. (Sawano et al., 2009b) explained in critical terms the logic behind the success story of the dimpled surface, such as controlling of wear debris and retaining lubrication.

Chapter 3.0 Materials and Methods

3.1 Introduction

Briefly, this section presents the materials and methods used for the study. The study is further broken down into 4 parts. Part 1 involves sample preparation, part 2 explains the technique use for dimple production, part 3 explains the methods used for surface characterization and finally tribology experiments.

3.2 Sample Preparation

Pure alumina oxide (99.6% Al_2O_3) plate at size of of 90×65×6 mm^3 and rod at diameter of 6.35 mm × 152.4 mm were bought from AdValue Technology (Tucson, USA). This type of ceramic is known for its high hardness, low friction, low wear and bio-compatibility. The chemical composition and engineering properties of this material are shown in Table 3.1 and Table 3.2 respectively. The plate and rod have to be prepared according to the sample specifications of the tribology machine (TR-281-M8). The new dimension for the plate is 15×15×6 mm^3 and 6. 35 mm (Ø) × 6mm for rod Figure 3.1a. A diamond cutter (IsoMet® 5000 Linear Precision Saw, BUEHLER) Figure 3.1b was used to cut the samples. The diamond blade speed was set to 4,000 rpm and feed rate at 2.5 mm/min (optimised rate). Each sample went through a series of polishing processes in order to achieve a mirror finish.

Table 3.1: Chemical Composition of the selected material

Chemical Composition (%)	Al_2O_3	>99.6
	SiO_2	<0.1
	Fe_2O_3	<0.05
	R_2O	<0.1

Table 3.2: Engineering properties of the selected material

	Units of measure	Value
Density	gm/cc (lb/ft^3)	>3.8
Porosity	% (%)	<0.5
Flexural Strength	MPa ($lb/in^2 \times 10^3$)	379
Elastic Modulus	GPa ($lb/in^2 \times 10^6$)	375
Shear Modulus	GPa ($lb/in^2 \times 10^6$)	152
Bulk Modulus	GPa ($lb/in^2 \times 10^6$)	228
Poisson's Ratio	-	0.22
Compressive Strength	MPa ($lb/in^2 \times 10^3$)	2600
Tensile Strength, 25^0C	MPa ($lb/in^2 \times 10^3$)	275
Hardness	Kg/mm^2	1440
Thermal Conductivity	W/m^0k ($BTU\text{-}in/ft^2 \times hr^0F$)	35
Coefficient of Thermal Expansion	$10^{-6}/^0C$ ($10^{-6}/^0F$)	8.4
Specific heat	J/Kg^0K (Btu/lb^0F)	880
Dielectric Strength	Ac-kv/mm (volts/mil)	16.9
Dielectric Constant	@1 MHz	9.8
Dissipation Factor	@1 MHz	0.0002

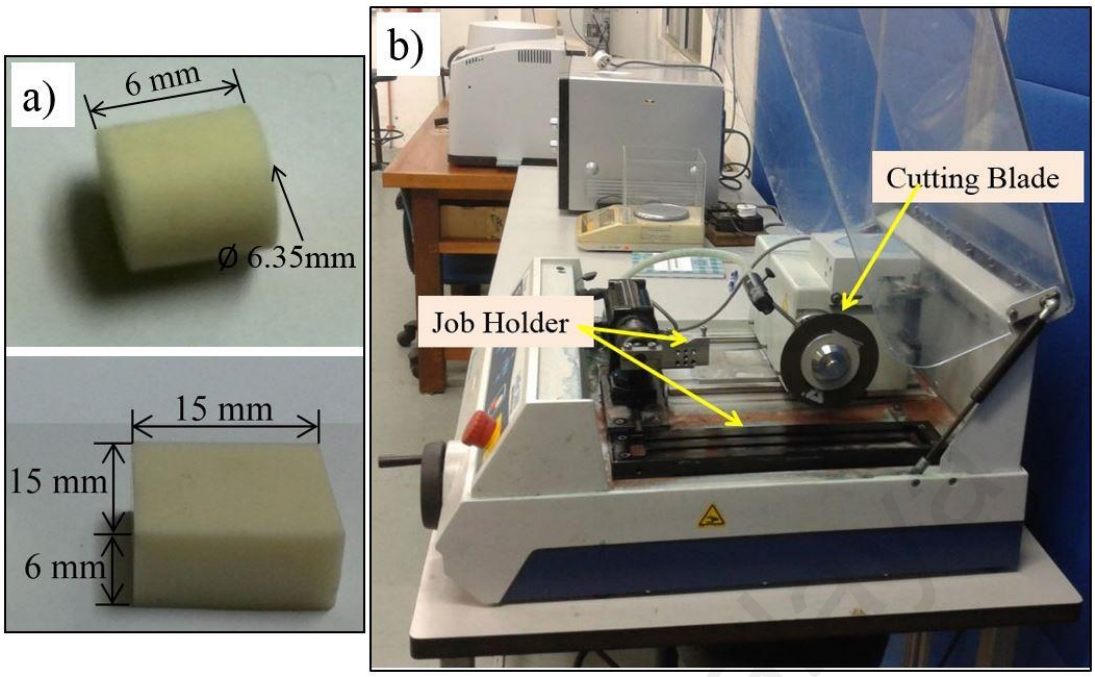

Figure 3.1: A) Pure alumina oxide (99.6% Al_2O_3) with dimension, b) Diamond cutter

Considering alumina oxide is a hard material, a diamond grinding disc (30µm) was used for initial polishing. With an adequate supply of water, the grinding process lasted 15 minutes with the grinding wheel set at 200 rpm for every sample. Figure 3.2 shows the polishing grinding machine. This is followed by sequential polishing with 9µm, 6µm, 1µm and 0.05 µm diamond polycrystalline suspensions (DPS). Every step with DPS lasted 10 minutes where the DPS supplied at 4/5 second interval in the form of drop, and the grinding wheel speed was set at 200 rpm.

Figure 3.2: Polishing grinding machine used for polishing

3.3 Dimple Fabrication

The key parameters for this experiment are the dimple array patterns and dimple profile, because it was previously reported that these parameters affect the tribology of a system (A Amanov et al., 2012; Auezhan Amanov et al., 2013; Andersson et al., 2007; Brizmer et al., 2003; Byun et al., 2010; Cho et al., 2011). 3 types of dimple array patterns were chosen for this study. The fixed variables in this study are the diameter of the dimple, dimple depth and pitch (centre distance between two dimples). Table 3.3 summaries the dimple parameters. CATIA software was used to draw the dimple array patterns (Figure 3.3). These design were later programmed into the CNC machine assisted micro drilling machine (Mikrotools DT110, Singapore) (Figure 3.4)

Table 3.3: Dimple parameters

Samples	Diameter, D (µm)	Depth, h (µm)	Aspect ratio, λ=D/h	Pitch , (µm)	*Dimple density,A(%)	Total no. of dimples
Non-dimpled	0	0	-	0	-	0
1: D300-P5	300	30	0.1	1000	5	121
2 :D300-P10	300	30	0.1	550	10	225
3: D300-P15	300	30	0.1	400	15	324
4: D400-P5	400	30	0.075	1800	5	49
5: D400-P10	400	30	0.075	1200	10	100
6: D400-P15	400	30	0.075	900	15	144

* A% = $\frac{total\ dimple\ \ area}{total\ surface\ area} \times 100$ (Kim et al., 2014)

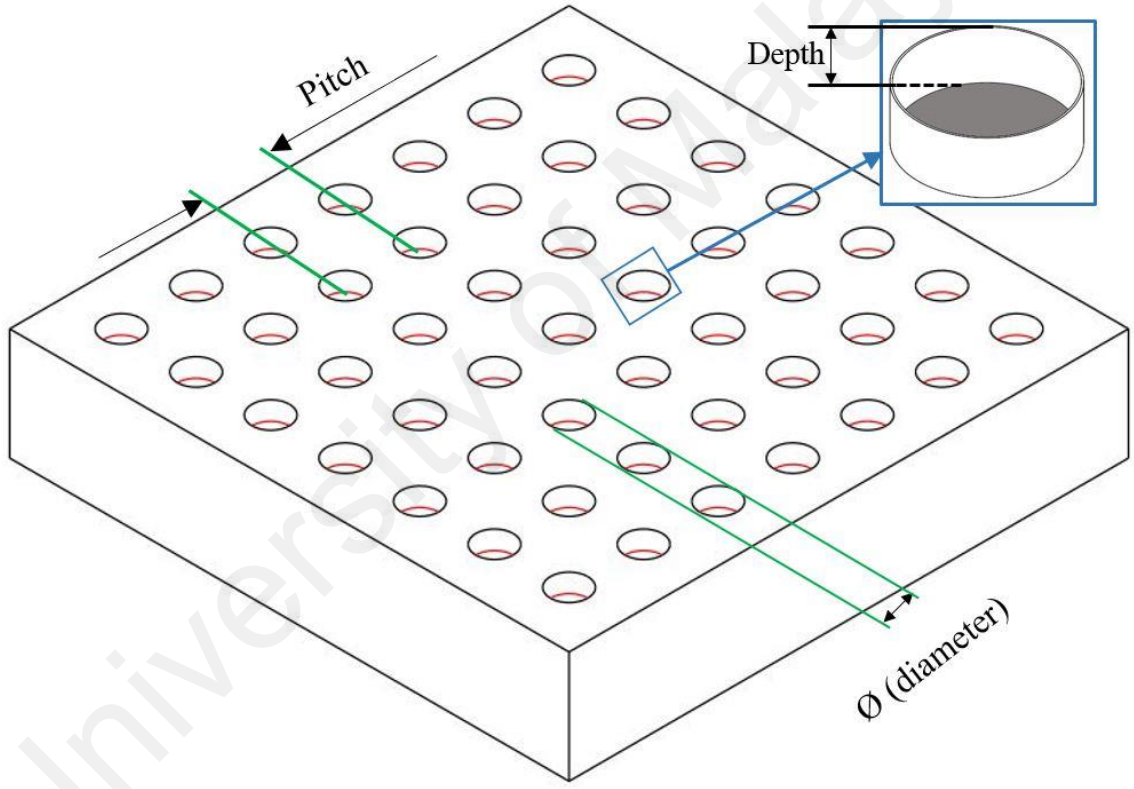

Figure 3.3: Schematic diagram of the dimple array patterns drawn using CATIA software

Figure 3.4: CNC assisted micro drilling machine

For this study, diamond drill bits (UKAM Industrial Superhard Tools, U.S.) were used. The polished alumina disks were placed inside the CNC machine. For effective machining, spindle speed and feed rate were set at 55,000 rpm and 334 mm/min respectively as per supplier recommendation. To preserve the life time of the drill bit, only 10 µm feed was used in every step during fabrication.

3.4 Surface characterization

3.4.1 Roughness:

The sample surface roughness Ra, was measured using a 3D optical profiler (Alicona Infinite focus). An average of ten readings were collected from each sample. For the dimpled surface, the roughness were measured between the areas of dimple (showed in Figure 3.5).

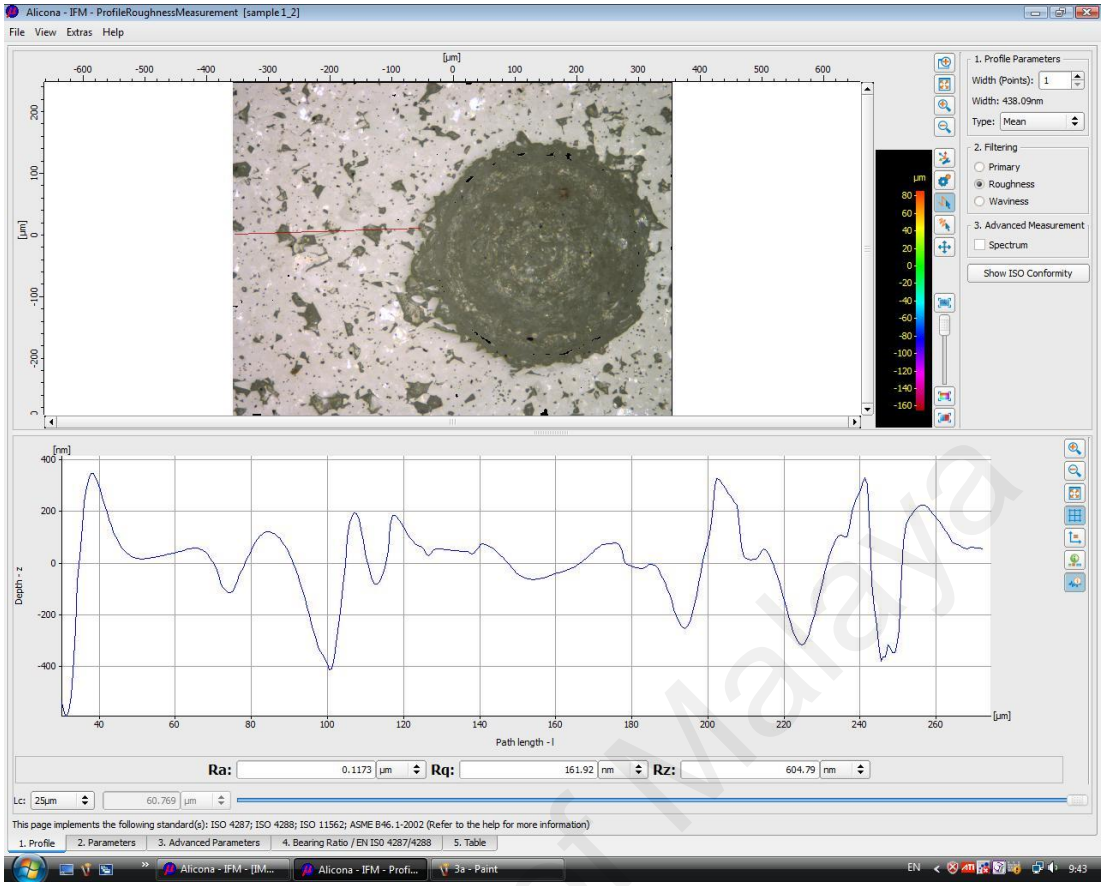

Figure 3.5: Surface roughness pattern for the sample by 3-D optical surface profiler

3.4.2 Dimple profile measurement:

The dimple diameter, pitch and depth were measured by a 3D optical profiler. An average of 10 readings were collected from each sample. Field emission scanning electron microscopy (FESEM; AURIGA, Zeiss Singapore) was used to look at the dimple morphology.

3.4.3 Evaluation of fabrication contamination:

Friedrich (Friedrich, 2002) mentioned the possible surface integrity caused by the cutting process, and unexpected wear debris (chips) generated which may not be completely removed from the dimple. Therefore, samples are washed with 10%

sulphuric acid, distilled water and ultrasonic cleaner, and then tested with X-ray diffraction (XRD) (Philips X'pert MPD PW3040, Singapore) and EDS (SEM; Philips XL40). The XRD pattern of the sample is then compared to that of Al_2O_3 (JCPDS card 46-0306). EDS also employed to determine the presence of any other foreign particles generated during the fabrication process.

3.4.4 Mechanical properties:

3.4.4.1 Hardness

A Vickers micro indenter (HVS-1000) was used to measure the hardness of the dimpled and non-dimpled surface area. Seven selected areas were indented for each sample. And for dimpled surface, each selected area was further divided in 3 zones, such as, A- very near to the periphery of the dimple; B-50 μm apart from the periphery of the dimple; C-100 μm apart from the periphery of the dimple (showed in Figure 3.6). The load was set to 980.7 mN for duration of 10 sec. The average data showed the micro hardness of the sample.

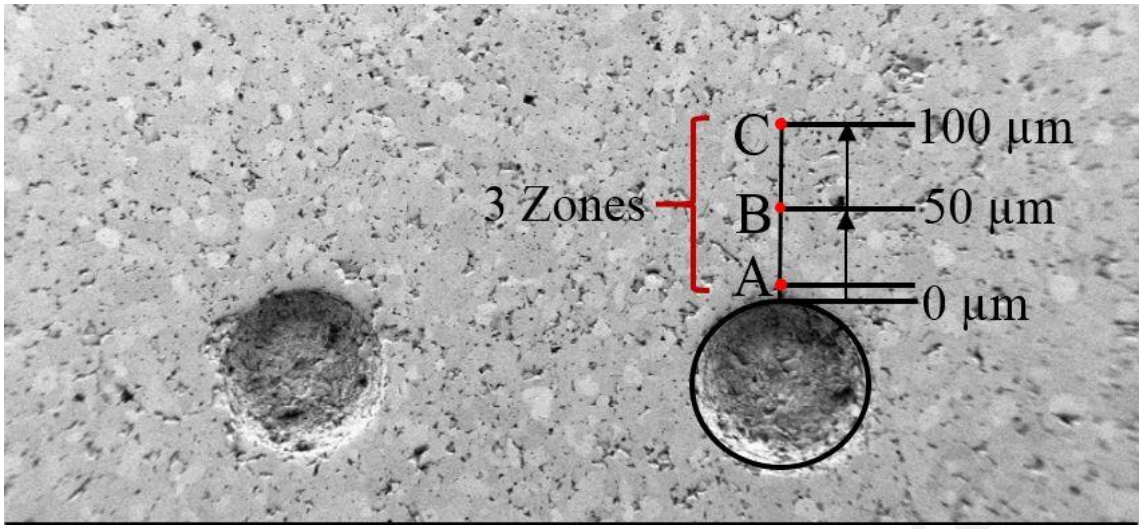

Figure 3.6: FESEM micrograph of dimpled surface with defined 3 zones for hardness tests. A-very near to the periphery, B-50 µm apart from the periphery of the dimple and C-100 µm apart from the periphery of the dimple

3.4.4.2 Residual stress

Residual stresses are stresses that remain in a solid material after the original cause of the stresses have been removed. Many researchers have reported the feasibility of X-ray diffraction method to measure the residual stress of the material (Arafat et al., 2013; Khan et al., 2007; Khan et al., 2005, 2006). In our study, we have used an X-ray diffractometer (XRD: PA Nalytical Empyrean) to measure the residual stress generated by CNC drilling. The xrd-$\sin^2\psi$ technique was employed using CuKα radiation (0.1540598 nm) at 40 kV and 40 mA. The different tilt angles (ψ) were employed ranging from -40º to 40º by a computer controlled Omega-goniometer. Residual stress calculation are shown in appendix A.

3.4.5 Wettability:

The wettability measurement determines the hydrophobic or hydrophilic property of the sample surface. Wettability was measured by water contact angle measurement with a goniometer (OCA15EC, Dataphysics Instrument, Germany). The static sessile drop method was used with a single drop of 2µl water on the surface. High resolution cameras and software were used to capture and analyse the contact angle. For dimpled surfaces, the drop was put between the dimples and all the experiments were repeated 10 times, with mean values of those readings showing the wettability of the surface.

3.4.6 Tribology testing:

3.4.6.1 Contact pressure estimation:

The Hertzian contact theory was used to calculate the maximum contact pressure (Hertz, 1982; Tay et al., 2011). The Hertz's equation to calculate the maximum contact pressure along the center line of the contact area of cylindrical and planar contact is given as:

$$P_{max} = \frac{2F}{\pi b L} \quad \ldots\ldots\ldots\ldots\ldots\ldots\ldots\ldots\ldots\ldots\ldots\ 3.1$$

Where, P_{max} is the maximum contact pressure, F is the normal load applied to the surface, L is the length of contact, and b is the half width of the rectangular contact area which is calculated as follows:

$$b = \sqrt{\frac{4F\left[\frac{1-\vartheta_1^2}{E_1}+\frac{1-\vartheta_2^2}{E_2}\right]}{\pi L\left(\frac{1}{R_1}+\frac{1}{R_2}\right)}} \quad \ldots\ldots\ldots\ldots\ldots\ldots\ldots\ldots\ldots 3.2$$

$\vartheta_{1,2}$, $E_{1,2}$ and $R_{1,2}$ are the Poisson's ratio, elastic modulus and radius of curvature (for planer surface R= α) of the two contacting materials respectively. Figure 3.7 shows the schematic diagram of a typical contact arrangement of a tribology setup.

For calculating maximum contact pressure, the mean elastic modulus of Alumina was determined as 375 GPa (for plate and rod), poisson's ratio was taken as 0.22 (for plate and rod) and the curvature of the radius of the pin (rod) was 3.175 mm and the curvature of the plate specimen was infinite. The calculated result is listed in Table 3.4.

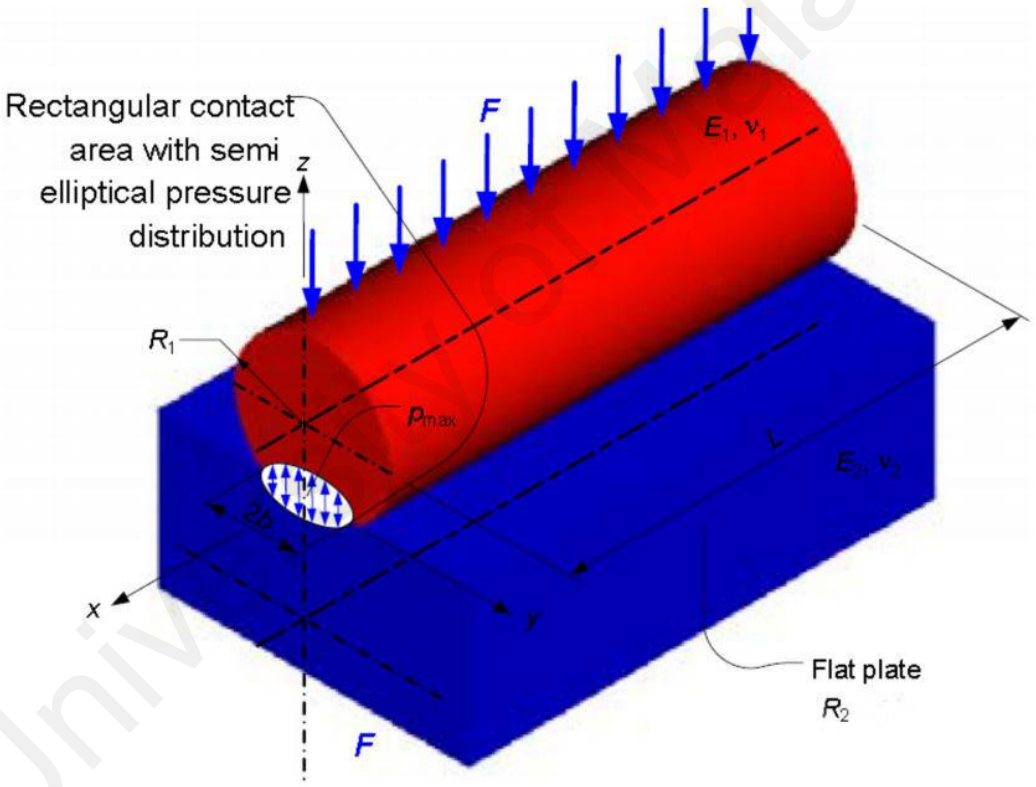

Figure 3.7: Contact demonstration of the tribology testing

3.4.6.2 Friction and wear measurement:

The tribology test was conducted using a tribometer (TR 283 Series, DUCOM, Bangalore, India) with modified flat-on-line contact configuration. Reciprocating housing drive with electrical motor provide the reciprocating sliding motion. The form of sliding speed was rectangular. Load sensor attached with the specimen holder was used to measure the frictional force. For data acquisition, WinDucom software installed on computer. The test sequence on the machine based on temperature and test duration, frequency and amplitude was controlled by the WinDucom software. Pin sample (Al_2O_3 rod) was installed into a metallic holder, and restricted to zero degrees of freedom. The centre of the pin holder was loaded in the direction normal to the Al_2O_3 disk located beneath the pins. The pin was moving along in the reciprocating direction in which the disk was fixed. Figure 3.8 shows the experimental setup.

The experimental parameters were selected based on a simulated hip joint, defined in terms of contact pressure, speed, and lubrication. Table 3.4 lists the experimental conditions for each type of tests. Applied loads were calculated with the simulated contact pressure of the hip joint (Mischler et al., 2012; Widmer et al., 2001). The stroke length was fixed and the frequency 5, 10, 15 and 20 Hz gave the sliding speed 20, 40, 60, 80 mm/sec respectively. Each test was carried out for 180 minutes and an average friction coefficient was calculated for every 900 cycles. Immediately before testing, each sample (pin and disk) put into an ultrasonic cleaner in iso-propanol for 10 min to remove any debris. Prior to, and at after testing, the cleaned disks were dried and allowed to stand in an environment with controlled humidity and temperature for 48 h, after which they were weighed to an accuracy of ±10µg. Each disk was weighed five times and the average value taken, allowing the weight loss over a period of testing to be calculated. This weight loss was taken as wear of the samples. Finally an FESEM

analysis was carried out to check for any cracking on the sample surfaces due to sliding and wear debris characterization. For this experiments, bovine serum (HCL#SV30160.03; HyClone Fetal Bovine Serum (South America), Research Grade) was used as the lubricant. All the test were carried out in flooded condition of the samples with lubricant and each test repeated three times.

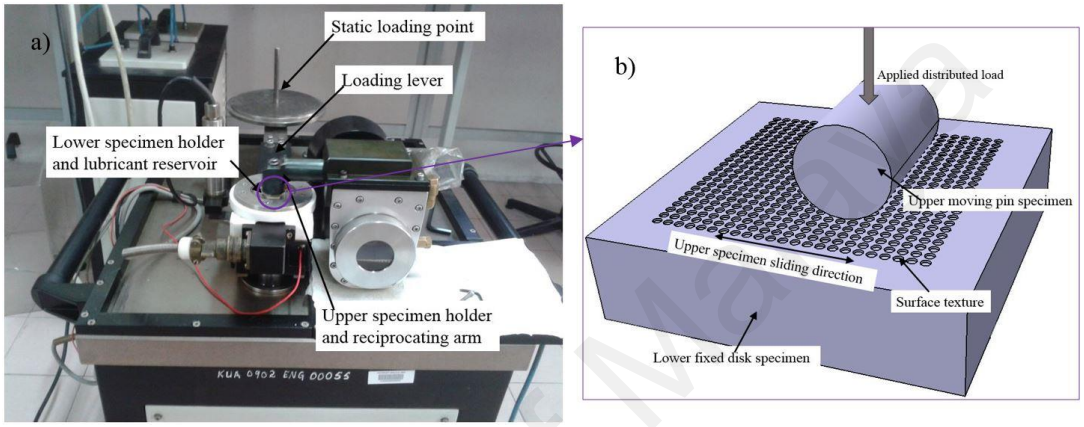

Figure 3.8: a) Reciprocating friction and wear machine; b) schematic diagram of loading and motion configuration of experimental setup.

Table 3.4: Tribology testing conditions

No.	Load (N)	Speed (mm/s)	Max. contact pressure (MPa)	Lubricant
1	10	20	181.45	Fetal bovine serum
2	15	20, 40, 60, 80	222.23	Fetal bovine serum
3	20	20	256.61	Fetal bovine serum

Chapter 4.0 Results & discussion

4.1 Surface characterization:

4.1.1 Surface roughness:

The measured average surface roughness (Ra) of the Al_2O_3 plate (dimpled or un-dimpled) was 0.12 ± 0.02 μm, indicating the prepared samples had a smooth surface. The very small standard error measurement of the samples shows that almost all the samples had the same surface roughness Table 4.1.

Table 4.1: Surface roughness of the samples

Sample	Avg. of 10 data (μm)	S.T.D (μm)
Non-dimple	0.1224	0.0103
1: D300-P5	0.1112	0.0131
2 :D300-P10	0.1220	0.0184
3: D300-P15	0.1257	0.0136
4: D400-P5	0.1204	0.0107
5: D400-P10	0.1290	0.0182
6: D400-P15	0.1266	0.0144

4.1.2 Dimple profile:

Figure 4.1(a) displays a typical 3-dimensional image of a dimple produced by the 3D profilometer and through which the dimple diameter, depth and pitch were measured. Table 4.2 summarises the measured and theoretical values of the dimple diameter, depth and pitch. In general, the variation between the measured and theoretical values was not more than 5%. This confirms that the CNC micro machine can be used to produce micro dimples with accuracy. The ability of the CNC micro machine to control accurate replication of dimple parameters allows the production of a

high quality dimpled surface. The 2D morphologies of the dimple array patterns were confirmed by FESEM Images (Figure 4.1(b)).

Table 4.2: Comparison of dimple parameters of setting and measured values (all dimensions are in μm)

Sample	Diameter (Setting value)	Diameter (Measured value)	Depth (Setting value)	Depth (Measured value)	Pitch (Setting value)	Pitch (Measured value)
D300-P5	300	311.61±6.939	30	33.8±1.6	1000	1021.63±25.26
D300-P10	300	311.61±6.939	30	33.8±1.6	550	536.95±20.26
D300-P15	300	311.61±6.939	30	33.8±1.6	400	413.05±19.66
D400-P5	400	409.20±3.8422	30	34.52± 2.11	1800	1816.83±24.50
D400-P10	400	409.20±3.8422	30	34.52± 2.11	1200	1211.91 ± 4.87
D400-P15	400	409.20±3.8422	30	34.52± 2.11	900	915.87±14.35

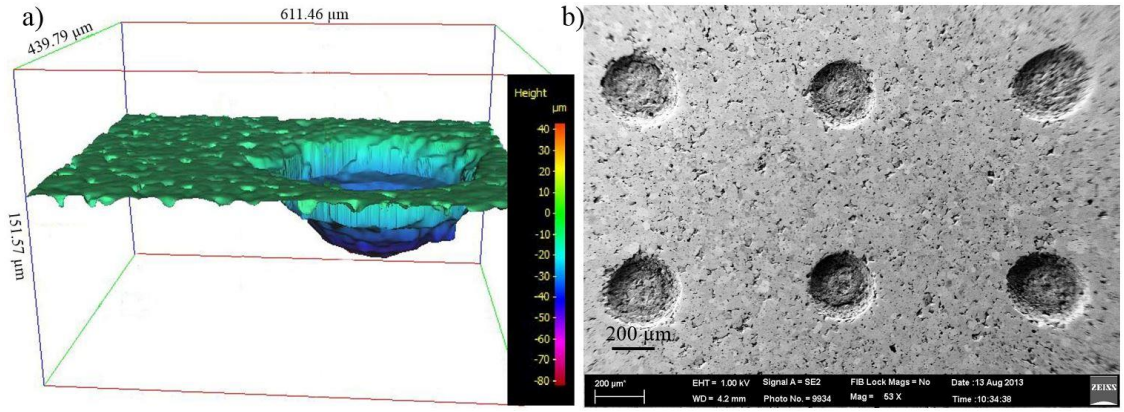

Figure 4.1: a) 3D image of dimpled surface produced by 3D optical profilometer b) 2D image of dimpled surface produced by FESEM

4.1.3 Fabrication contamination

The results of the wear debris (chips) tests were likewise supportive of the manufacturing method. The XRD pattern from the cleaned sample is shown in Figure 4.2, which coincides with that of aluminium oxide in the JCPDS card of 46-0306. Based on the XRD result, we conclude that there are no other foreign particle produced or remaining on the surface of the sample. The EDS pattern also showed no other foreign particle inside the dimple in Figure 4.3.

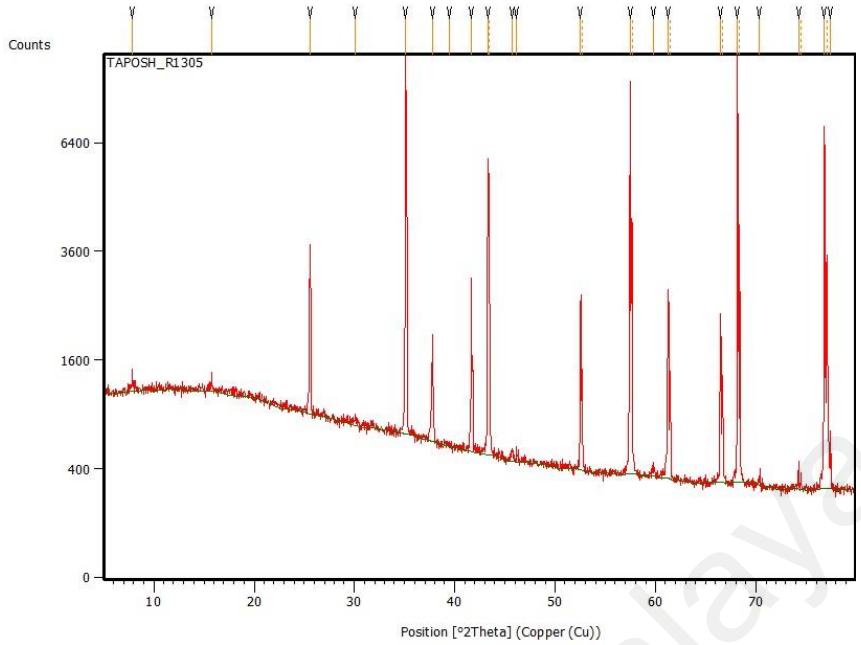

Figure 4.2: XRD pattern of the dimpled surface

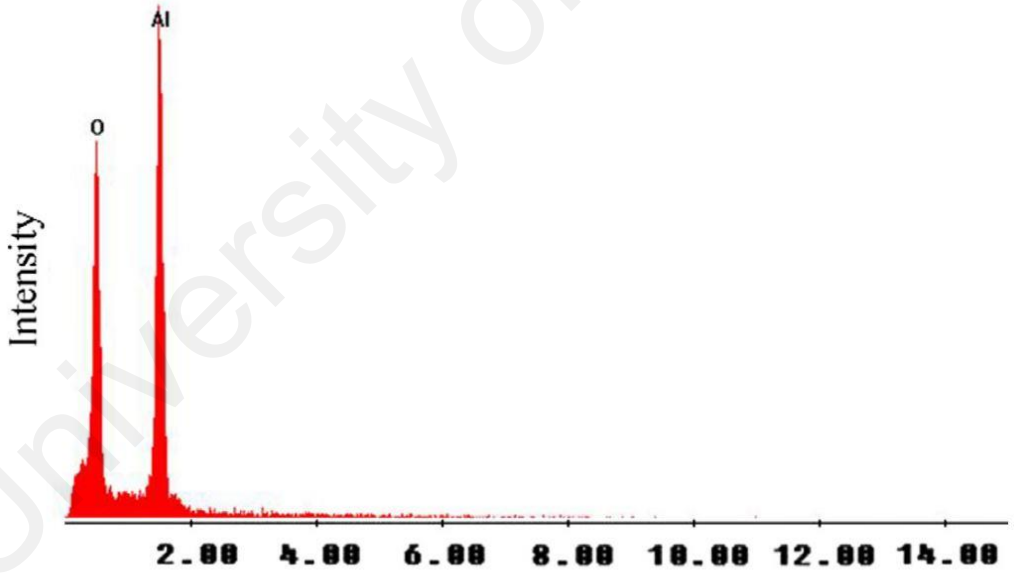

Figure 4.3:EDS pattern of the selected area inside the dimpled surface

4.1.4 Mechanical properties:

4.1.4.1 Hardness:

The average micro hardness for the non-dimple area was measured at 18.93 GPa and the average micro hardness for the dimple area was found to be slightly lower, at 18.06 for dimple with 300 µm diameter and 18.10 GPa for dimples with 400 µm diameter. The micro hardness very near to the dimple (in Figure 3.6position A) was a little bit lower that than 100 µm from the dimple periphery (Figure 3.6 position C). For the dimpled surface with 300 µm diameter dimples, the micro hardness calculated at positions A, B and C was measured as 17.5, 17.8 and 18.8 GPa respectively. This could be explained as a change of the grain micro structure due to the fabrication process and the geometric effect of the dimple. The geometric effect is that, a 300 µm deep hole is created on the surface so the area around to the hole might be weaker than the other surfaces. However the average micro hardness was near about same as the non-dimpled surface.

4.1.4.2 Residual stress

The residual stress on the dimpled surfaces was produced by the micro drilling fabrication process. The residual stress was found to be compressive stress. For the dimpled surface with 300 µm and 400 µm dimple diameters, it was -276 MPa (compressive) and -153 MPa (compressive). Compressive stress tends to reduce wear of the surfaces during friction (Alanazi et al., 2013).

4.1.5 Wettability

The wettability, in terms of water contact angle, for non-dimpled surfaces was 59º±3 and the dimpled surface was 62º±3 and 61º±3. The contact angle difference

between dimpled and non-dimpled was not significant. This shows that the samples are hydrophilic. The dimple fabrication did not alter the chemical property.

4.2 Tribology testing:

4.2.1 Effect of load with friction coefficient:

Friction coefficient is the one of fundamental tribological outputs and a lower friction coefficient is much desirable for artificial hip joints. The present study revealed significant differences in friction coefficient profiles among the experimental specimens at different loads and speeds. Figure 4.4, Figure 4.5 and Figure 4.6 shows the friction coefficient profiles of the experimental surfaces at contact pressures of 181.45, 222.23, and 256.61 MPa respectively, applying normal loads of 10, 15 and 20 N. Velocity was maintained at medium walking speed (20 mm/s)(Mischler et al., 2012; Widmer et al., 2001).

Overall all the dimple samples exhibited lower friction coefficient profiles compared to non-dimple samples. By the end of 54,000 cycles, under at normal load of 10 N, it was clearly demonstrated that the friction coefficient is affected by the dimple density. Both D300-P15 and D400-P15 samples show the lowest friction coefficient, which is 0.11(D300-P15) and 0.1(D400-P15) respectively (Figure 4.4). Both samples have similar dimple density. This results suggest the effect of dimple area ratio on the friction coefficient behaviour. However at higher loads or 15N and 20N the friction coefficient was greatly reduced by the sample having a bigger dimple diameter and density. D400-P15, which has the biggest dimple diameter and highest dimple density produced the lower friction coefficient (Figure 4.5, Figure 4.6). It is notable that all samples exhibited similar trends in response to load at both 15 and 20N (Figure 4.5, Figure 4.6), compared to non-dimple surfaces.

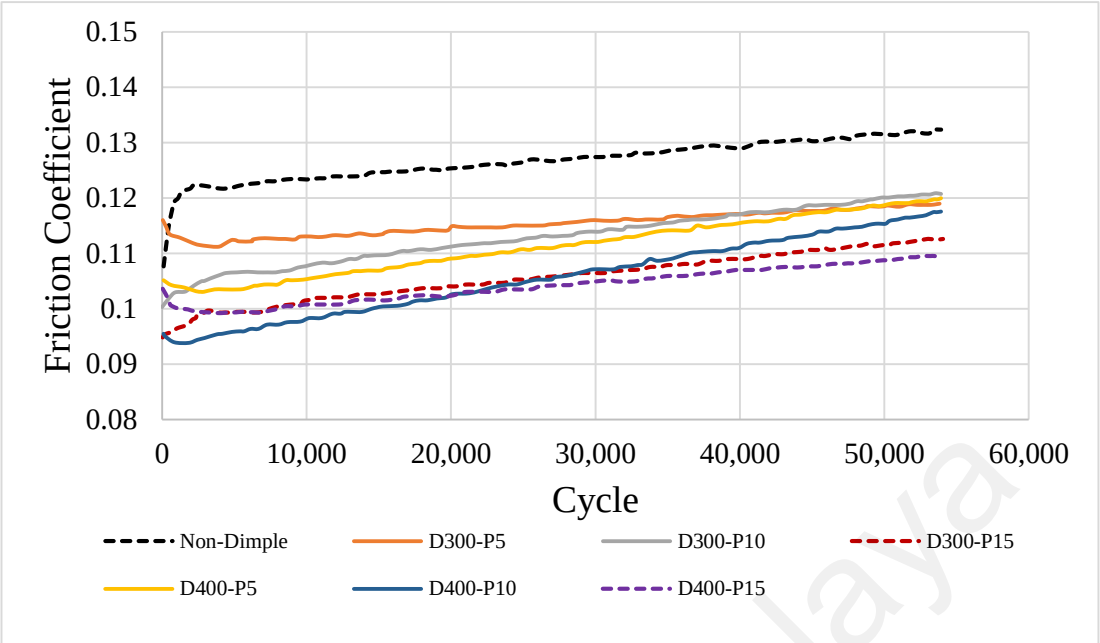

Figure 4.4: Frictional coefficient profile at sliding speed 20 mm/s. with 10 N load

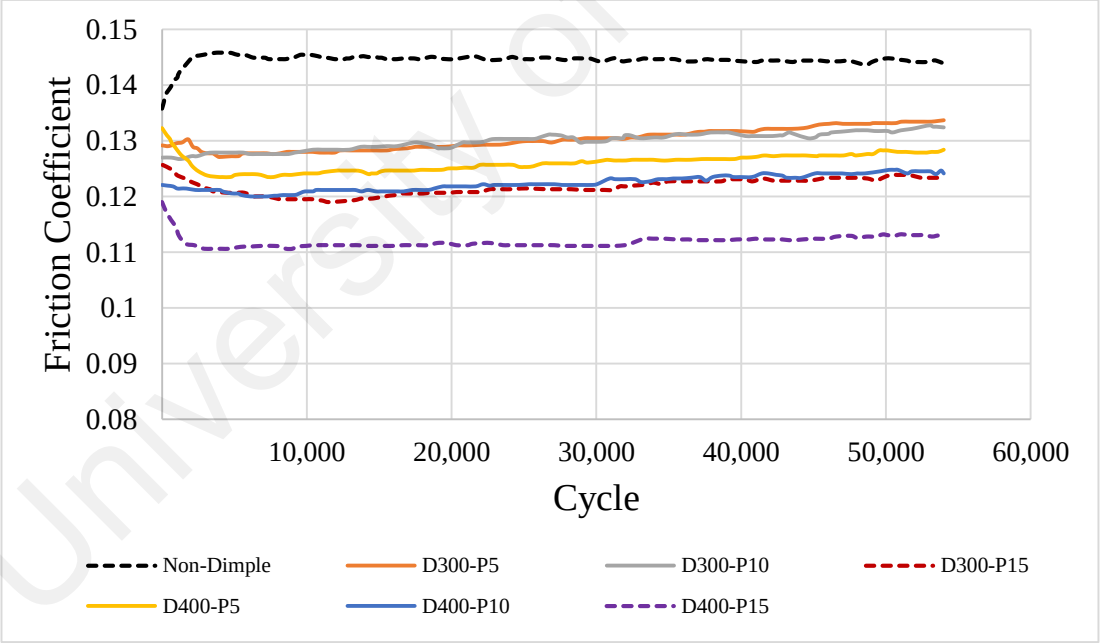

Figure 4.5: Frictional coefficient profile at sliding speed 20 mm/s with 15 N load

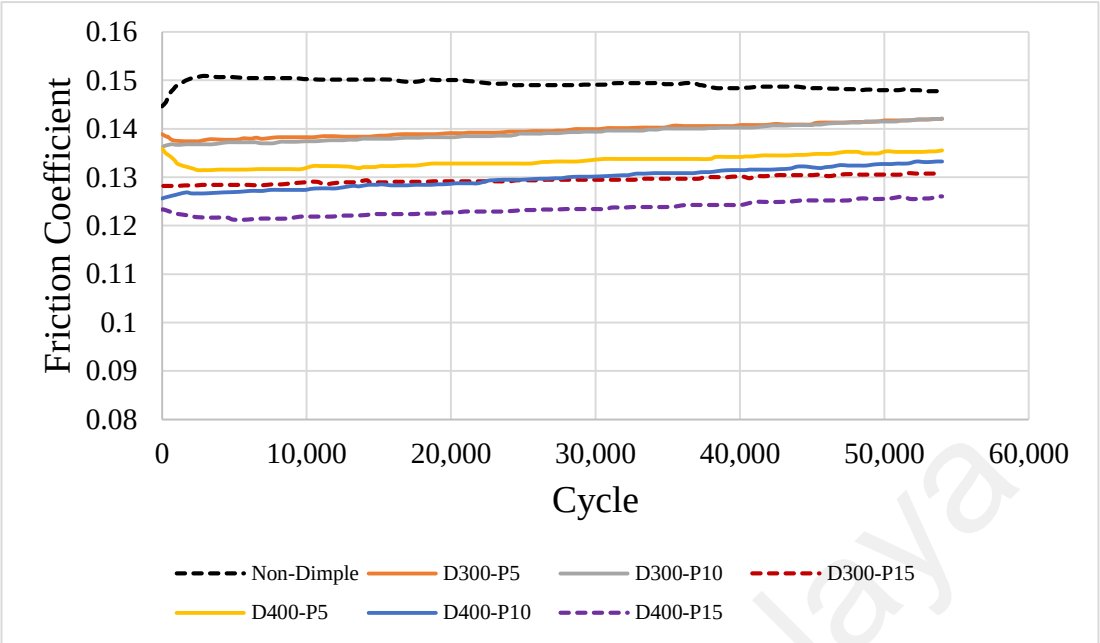

Figure 4.6: Frictional coefficient profile at sliding speed 20 mm/s. with 20 N load

Overall, the non-dimple samples produced the highest friction, and the values increases with the applied load (A Amanov et al., 2012; Wakuda et al., 2003). With the applied load 10N, at the beginning average friction coefficient was 0.108 and at the end of the cycle it was 0.132 for non-dimple samples. Where the increment of friction at the end of the cycle was 22%. For the same experimental condition sample D400-P15 showed the increment only 4.8%. Similarly other dimple samples showed small increment. This shows that samples with dimples have a better adaptability under changing load. It is worth noting that the contact pressure in hip joints is dynamic and depends on bodyweight and gait. Therefore, it can be speculated that samples with dimple surfaces are capable of providing lower and steady friction coefficients in dynamic loading conditions in hip joints. Our previous study (Roy et al., 2014) also revealed the importance of dimple surfaces. However, its effectiveness was limited to lower loads (10 N) because of the lower area ratio of dimpling (density 10%). As each of the dimples has the capability to generate hydrodynamic pressure, a higher area ratio

dimple surface certainly has a higher hydrodynamic pressure under sliding conditions, which contributes to lowering the friction coefficient.

4.2.2 Effect of speed on frictional behaviours:

The effect of sliding velocity on frictional behaviour was investigated. 15N was chosen as the fixed load and the tribometer was set at different sliding velocities, such as 20, 40, 60 and 80 mm/s. Figure 4.7 shows dependence between sliding speed and the mean value of the coefficient of friction, that dimple samples reduced friction coefficients. The confidence intervals are visible (the significance level was 0.05). In typical Stribeck diagram the coefficient of friction decreases as a function of velocity, reaches a minimum and increases thereafter. The region to the right of the minimum in the friction force curve corresponds to flood lubrication. However in our investigation it was found the maximum friction at higher speed and minimum friction at lower speed which also similar to the investigation by Liu et al. (Liu et al., 2010). In all cases non-dimple surface showed the maximum friction coefficient and dimple surface with higher area density (area density of 15%) showed the minimum friction coefficient. In Figure 4.7 it showed gradual increment of friction coefficient at the sliding speed 20 to 60mm/sec and then sharp increment at 80mm/sec. This can be explained, with the increase of sliding speed the lubricant squeeze out from the contact area of the sample. But for the dimple store the lubricant which supply lubricant during sliding. Adhesive force also can be the reason behind increase of friction coefficient. However results thus verified again that the dimple surface has great potential for reducing friction. These results reconfirmed the importance of dimple parameters, such as dimple diameter and dimple density. Clearly, a bigger dimple diameter and higher dimple density reduces friction coefficient. Samples with a higher dimple diameter have a smaller surface contact area, whereas samples with higher dimple density have more dimples, meaning more lubricant can be trapped in the dimples. This indirectly helps in lubricating the

samples. The benefit of having micro-dimples on the sample surface is obvious, and this is dependent on dimple diameter and dimple density.

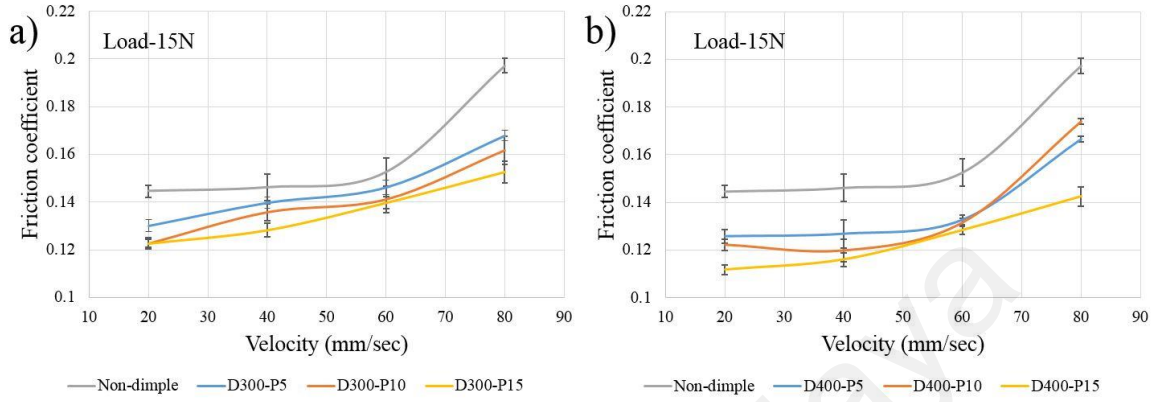

Figure 4.7: Friction coefficient produced by a) samples with dimple diameter of 300 µm and b) samples with dimple diameter of 400 µm

4.2.3 Wear and surface condition:

Wear is the main concern of artificial hip joints and a reduction of wear is the most desirable tribological outcome of a hip prosthesis. The dimple surface with a higher area ratio reduced friction coefficient significantly, however, it would not be wise to utilize it as a frictional material unless wear resistance is assured. Wear is a complex mechanism and it is partially related to friction coefficient. Moreover, a higher wear rate refers to a damage surface which actually increases friction coefficient to some extent. In this experiment, we considered weight loss of Al_2O_3 disk only for better consistency. It is to be noted that the weight loss was measured after completing the cycles under all types of applied load— 1,62,000 cycles for each of the samples. The experimental test of the weight loss of Al_2O_3 disk is presented in the Figure 4.8. D400-P15 has the lowest wear and followed by D300-P15, D300-P10, D400-P10, D300-P5, D400-P5 and non-dimple surfaces. The difference between the highest and lowest wear is 53% — which demonstrates an improved wear by the micro dimple surfaces technique. This result was

similar to the trend of the numerical simulation of Sawano et al. (Sawano et al., 2009a) and the experimental result of Ito et al. (Ito et al., 2000). Both of them investigated on metal-on-polyethylene whereas the present study focused on CoC hip joints. A controversial result was published by Zhou et al. (X. Zhou et al., 2012) which demonstrated an increased wear rate by using a dimple surface; the main limitation of that study was the large diameter of the dimple and area ratio was very low. This study also pointed out the low effectiveness of a modified surface which was fabricated with lower densities of dimples. FESEM image analysis was conducted after the friction tests to investigate the worn surface and size and shape of wear debris due to sliding of the test specimens. As shown in Figure 4.9 the only visible wear was fatigue wear and some grain pull-out wear found near the dimple edge. However wear due to grain pull out was found very rare. Most of the dimples were found unworn. Along with wear, the size and the shape of wear debris are important factors in the durability of the prosthesis. Cell proliferation, differentiation, and prostanoid are affected by the size, shape, and chemical composition of the particles. Nine et al. (Nine et al., 2014) concluded that nano-sized wear debris is more reactive to the surrounding tissue; however its toxicity is dose dependant. Figure 4.10, Figure 4.11 and Figure 4.12 show the morphology of wear debris filtered from used lubricant from the tribology test.

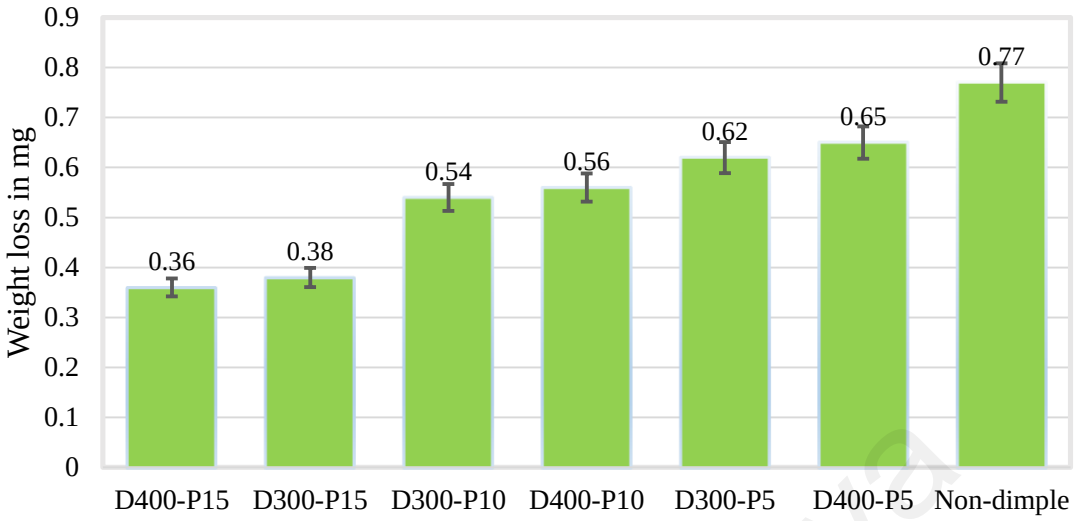

Figure 4.8: Comparison of mass loss for different samples. Error bar shows the standard deviation of the weight loss.

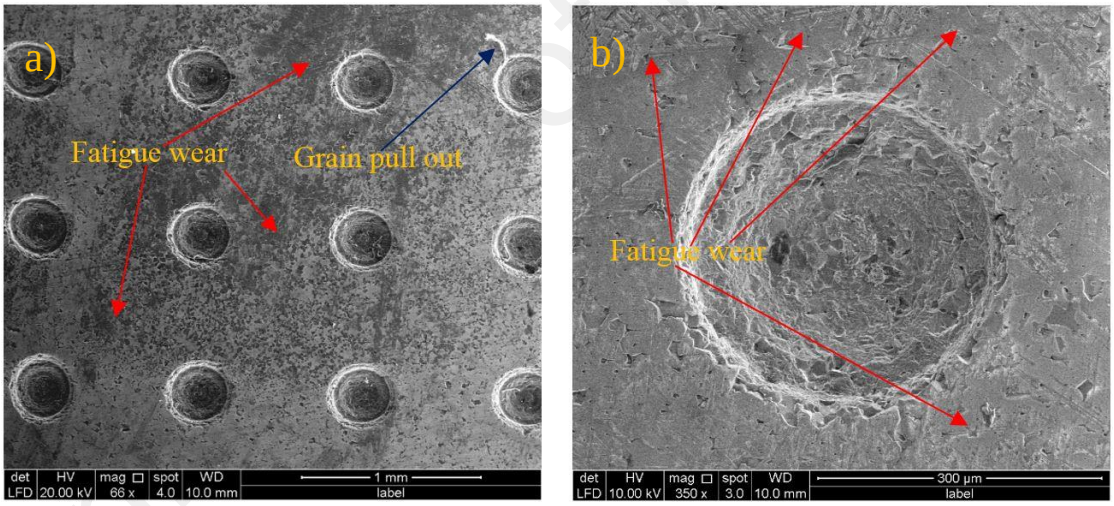

Figure 4.9: SEM images of the dimpled surface and collected wear debris after tribology testing. a) Image of wear track on the dimpled sample, b) Image of fatigue wear on a dimple sample after tribology test.

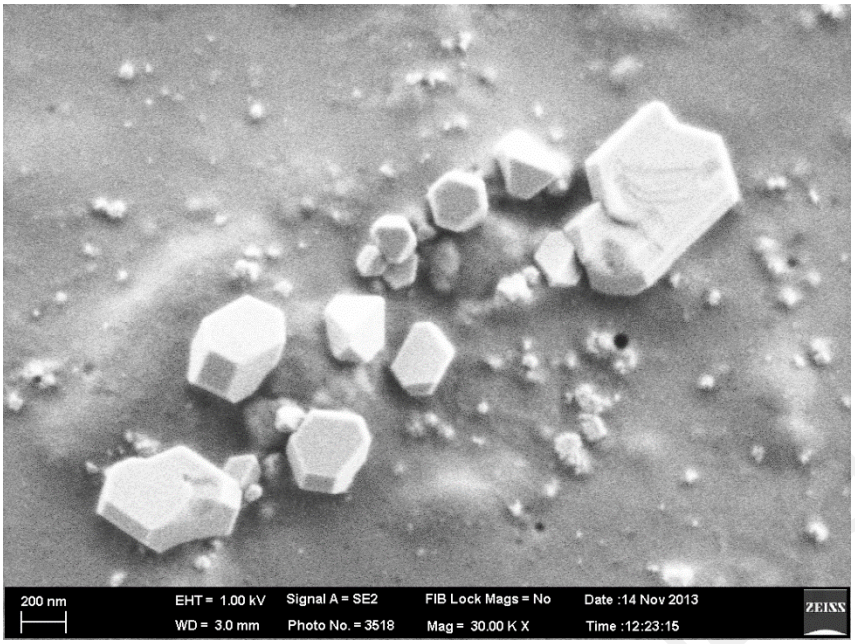

Figure 4.10: SEM images of the dimpled surface and collected wear debris after tribology testing. wear debris collected after tribology test from a non-dimple surface

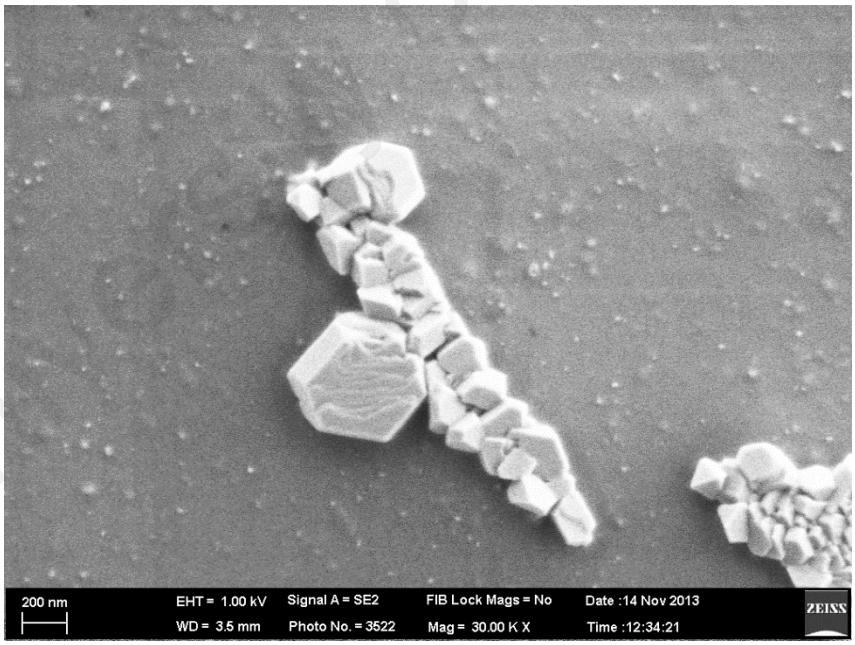

Figure 4.11: SEM images of the dimpled surface and collected wear debris after tribology testing from sample D300-P15

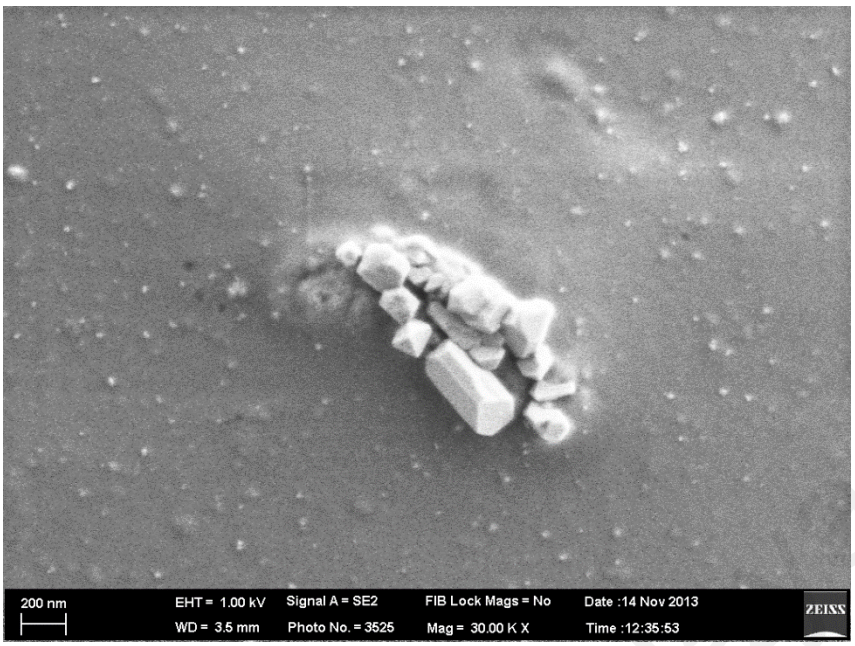

Figure 4.12: SEM images of the dimpled surface and collected wear debris after tribology testing from sample D400-P15.

From figure above, it is seen that the wear debris generated from the non-dimple specimens is typically bigger in size than that from non-dimple specimens. The cause behind the smaller size wear debris with dimple surface can described by surface continuity. For the non-dimple surface, the contact area throughout the sliding time found to be continuous. Whereas due to fabricating dimple the contact area was not continuous. This may be the cause of bigger wear debris for non-dimple surfaces with compare to dimple surface. However, this is random study of wear debris without following an appropriate protocol for wear debris separation and so the results are not yet conclusive in their detail. Nine et al. (Nine et al., 2014) concluded that ceramic wear debris greater than 500 μm is less reactive to the surrounding tissue, however its toxicity is dose dependant. The average size of wear debris was found to be approximately 600-700 nm for dimple configuration.

Chapter 5.0 Conclusion and Future work

5.1 Conclusion:

5.1.1 Dimple characterization:

A successful fabrication of Micro dimple array on Al_2O_3 surfaces revealed the feasibility of applying micro tools on ceramic surfaces. The key findings of this research are as follows:

i. CNC assisted micro drilling is a reliable process for fabricating micro dimple arrays with different geometries on ceramic surfaces. The dimple parameters were precisely characterized (diameter, depth, pitch), each with very low standard deviation, which means the fabrication process is repeatable.

ii. The average hardness was found to be 4.38% lower compared to the non-textured surface. The hardness was slightly lower near the dimple periphery but the outer surface hardness was almost the same as the no-dimpled surface. The induced residual stress was compressive (-276 MPa) at the centre of the dimple.

iii. There were not any detectable wear debris nor were there cutting chips found in the dimple holes.

5.1.2 Tribology:

The tribological effects of various geometric parameters with different dimple densities and diameters were investigated using a reciprocating tribometer under bovine serum lubrication. The comparison between dimple and non-dimple samples revealed that dimple samples reduced the frictional coefficient and wear in a simulated hip joint condition. The friction test revealed that the measured coefficient of friction for a

dimple surface with dimple diameter 400 µm, density 15% and depth 30 µm lowered the maximum coefficient of friction by 22% and wear 53%. The frictional coefficient varied with respect to velocity and load. At 15 N load, the dimple surfaces lowered the maximum coefficient of friction with compare to non-dimple surface. The wear debris were found in smaller size for dimple surface with compare to non-dimple surface. Therefore, after considering the coefficient of friction, wear, and wear debris storing capacity, we conclude that the micro dimple surface (profile: Ø400µm, depth 30µm and density 15%) has an improved tribological performance when compared to the polished surface.

5.2 Future work:

Future further studies can be conducted in following areas:

1. Film thickness measurement during sliding motion as film thickness is one of the key factors to understand in a lubrication mechanism.
2. Mechanical and biological characterization of wear debris.

References

Alanazi, Nayef M, El-Sherik, AM, Alamar, Saleh H, & Shen, Shouwen. (2013). Influence of Residual Stresses on Corrosion and Wear Behavior of Electrodeposited Nanocrystalline Cobalt-Phosphorus Coatings. *International Journal of Electrochemical Science, 8*, 10350 – 10358.

Amanov, A, Cho, IS, Pyoun, YS, Lee, CS, & Park, IG. (2012). Micro-dimpled surface by ultrasonic nanocrystal surface modification and its tribological effects. *Wear, 286*, 136-144.

Amanov, Auezhan, Pyun, Young Sik, Zhang, Bin, Park, Jeong Hyeon, & Nohava, Jiri. (2011). Preliminary study of the effect of micro-scale dimple size on friction and wear under oil-lubricated sliding contact. *Tribology Online, 6*(7), 284-290.

Amanov, Auezhan, & Sasaki, Shinya. (2013). A Study On The Tribological Characteristics Of Duplex–Treated Ti–6al–4V Alloy Under Oil–Lubricated Sliding Conditions. *Tribology International*. 64, 155 ‑ 163.

Andersson, P, Koskinen, J, Varjus, S etc, Gerbig, Y, Haefke, H, Georgiou, S, . . . Buss, W. (2007). Microlubrication effect by laser-textured steel surfaces. *Wear, 262*(3), 369-379.

Arafat, M. M., Haseeb, A. S. M. A., Dinan, B., & Akbar, S. A. (2013). Stress enhanced TiO2 nanowire growth on Ti–6Al–4V particles by thermal oxidation. *Ceramics International, 39*(6), 6517-6526.

Balla, Vamsi Krishna, Bodhak, Subhadip, Bose, Susmita, & Bandyopadhyay, Amit. (2010). Porous tantalum structures for bone implants: fabrication, mechanical and in vitro biological properties. *Acta biomaterialia, 6*(8), 3349-3359.

Ben Zaïda, Y. (2008). *Contribution à la conduite du changement du système entreprise.* Thèse de doctorat, Université Montpellier 2.

Bhattacharyya, B, Mitra, S, & Boro, AK. (2002). Electrochemical machining: new possibilities for micromachining. *Robotics and Computer-Integrated Manufacturing, 18*(3), 283-289.

Borghi, Aa, Gualtieri, E, Marchetto, D, Moretti, L, & Valeri, S. (2008). Tribological effects of surface texturing on nitriding steel for high-performance engine applications. *Wear, 265*(7), 1046-1051.

Brizmer, V, Kligerman, Y, & Etsion, I. (2003). A laser surface textured parallel thrust bearing. *Tribology Transactions, 46*(3), 397-403.

Bruzzone, AAG, Costa, HL, Lonardo, PM, & Lucca, DA. (2008). Advances in engineered surfaces for functional performance. *CIRP Annals-Manufacturing Technology, 57*(2), 750-769.

Byrne, G, Dornfeld, David, & Denkena, B. (2003). Advancing cutting technology. *CIRP Annals-Manufacturing Technology, 52*(2), 483-507.

Byun, Jung Won, Shin, Hong Shik, Kwon, Min Ho, Kim, Bo Hyun, & Chu, Chong Nam. (2010). Surface texturing by micro ECM for friction reduction. *International Journal of Precision Engineering and Manufacturing, 11*(5), 747-753.

Cho, MH, & Park, Sangil. (2011). Micro CNC surface texturing on polyoxymethylene (POM) and its tribological performance in lubricated sliding. *Tribology International, 44*(7), 859-867.

Choudhury, Dipankar, Walker, Robert, Roy, Taposh, Paul, Sweety, & Mootanah, Rajshree. (2013). Performance of honed surface profiles to artificial hip joints: An experimental investigation. *International Journal of Precision Engineering and Manufacturing, 14*(10), 1847-1853.

Choudhury, Dipankar, Walker, Robert, Shirvani, Ayoub, Mootanah, Rajshree, & Chelmsford, UK. (2013). The Influence of Honed Surfaces on Metal-on-Metal Hip Joints. *Tribology Online, 8*(3), 195-202.

Chouquet, C., Gavillet, J., Ducros, C., & Sanchette, F. (2010). Effect of DLC surface texturing on friction and wear during lubricated sliding. *Materials Chemistry and Physics, 123*(2), 367-371.

Costa, HL. (2005). Modification of Surface Topography: Manufacturing Methods and Applications. *PhD Thesis, University of Cambridge*, 240.

Costa, HL, & Hutchings, IM. (2007). Hydrodynamic lubrication of textured steel surfaces under reciprocating sliding conditions. *Tribology International, 40*(8), 1227-1238.

Costa, HL, & Hutchings, IM. (2009). Development of a maskless electrochemical texturing method. *Journal of Materials Processing Technology, 209*(8), 3869-3878.

Dhanik, Sandeep, Joshi, SS, Ramakrishnan, N, & Apte, PR. (2005). Evolution of EDM process modelling and development towards modelling of the micro-EDM process. *International journal of manufacturing technology and management, 7*(2), 157-180.

Dhanik, Sandeep, & Joshi, Suhas S. (2005). Modeling of a single resistance capacitance pulse discharge in micro-electro discharge machining. *Journal of manufacturing science and engineering, 127*(4), 759-767.

Dhobe, Shirish D, Doloi, B, & Bhattacharyya, B. (2011). Analysis of surface characteristics of titanium during ECM. *International Journal of Machining and Machinability of Materials, 10*(4), 293-309.

Dowson, D, McNie, CM, & Goldsmith, AAJ. (2000). Direct experimental evidence of lubrication in a metal-on-metal total hip replacement tested in a joint simulator. *Proceedings of the Institution of Mechanical Engineers, Part C: Journal of Mechanical Engineering Science, 214*(1), 75-86.

Dubey, Avanish Kumar, & Yadava, Vinod. (2008). Laser beam machining—a review. *International Journal of Machine Tools and Manufacture, 48*(6), 609-628.

Findlay, David M, Welldon, Katie, Atkins, Gerald J, Howie, Donald W, Zannettino, Andrew CW, & Bobyn, Dennis. (2004). The proliferation and phenotypic expression of human osteoblasts on tantalum metal. *Biomaterials, 25*(12), 2215-2227.

Fleischer, J, Masuzawa, T, Schmidt, J, & Knoll, M. (2004). New applications for micro-EDM. *Journal of Materials Processing Technology, 149*(1), 246-249.

Friedrich, CR. (2002). Micromechanical machining of high aspect ratio prototypes. *Microsystem technologies, 8*(4-5), 343-347.

Gao, L., Yang, P., Dymond, I., Fisher, J., & Jin, Z. (2010). Effect of surface texturing on the elastohydrodynamic lubrication analysis of metal-on-metal hip implants. *Tribology International, 43*(10), 1851-1860.

Hertz, H. (1982). On the contact of elastic solids. *J. Reine. angew. Math*(92), 156–171.

Ho, KH, & Newman, ST. (2003). State of the art electrical discharge machining (EDM). *International Journal of Machine Tools and Manufacture, 43*(13), 1287-1300.

Ho, KH, Newman, ST, Rahimifard, S, & Allen, RD. (2004). State of the art in wire electrical discharge machining (WEDM). *International Journal of Machine Tools and Manufacture, 44*(12), 1247-1259.

Hu, T. C., Hu, L. T., & Ding, Q. (2012). Effective solution for the tribological problems of Ti-6Al-4V: Combination of laser surface texturing and solid lubricant film. *Surface & Coatings Technology, 206*(24), 5060-5066.

Huaiqian, Bao, Jiawen, Xu, & Ying, Li. (2008). Aviation-oriented Micromachining Technology—Micro-ECM in Pure Water. *Chinese Journal of Aeronautics, 21*(5), 455-461.

Huang, H, Zhang, Hong, Zhou, L, & Zheng, HY. (2003). Ultrasonic vibration assisted electro-discharge machining of microholes in Nitinol. *Journal of micromechanics and microengineering, 13*(5), 693.

Huang, W., Jiang, L., Zhou, C. X., & Wang, X. L. (2012). The lubricant retaining effect of micro-dimples on the sliding surface of PDMS. *Tribology International, 52*, 87-93.

Huang, Wei, Jiang, Liang, Zhou, Chuanxi, & Wang, Xiaolei. (2012). The lubricant retaining effect of micro-dimples on the sliding surface of PDMS. *Tribology International, 52*, 87-93.

Illgen II, Richard Lynn, Bauer, Lia M, Hotujec, Bryan T, Kolpin, Sarah E, Bakhtiar, Aleem, & Forsythe, Todd M. (2009). Highly crosslinked vs conventional polyethylene particles: relative in vivo inflammatory response. *The Journal of arthroplasty, 24*(1), 117-124.

Ingham, Eileen, & Fisher, John. (2005). The role of macrophages in osteolysis of total joint replacement. *Biomaterials, 26*(11), 1271-1286.

Ito, H., Kaneda, K., Yuhta, T., Nishimura, I., Yasuda, K., & Matsuno, T. (2000). Reduction of polyethylene wear by concave dimples on the frictional surface in artificial hip joints. *The Journal of Arthroplasty, 15*(3), 332-338.

Jahan, MP, Rahman, M, & Wong, YS. (2011). A review on the conventional and micro-electrodischarge machining of tungsten carbide. *International Journal of Machine Tools and Manufacture, 51*(12), 837-858.

Jahan, MP, Wong, YS, & Rahman, M. (2009). A study on the quality micro-hole machining of tungsten carbide by micro-EDM process using transistor and RC-type pulse generator. *Journal of Materials Processing Technology, 209*(4), 1706-1716.

Jameson, E.C. (2001). Description and development of electrical discharge machining (EDM). *Electrical Discharge Machining, Society of Manufacturing Engineers, Dearbern, Michigan*, 12.

Jeon, D. H., Kim, B. H., & Chu, C. N. (2006). Micro machining by EDM and ECM. *Journal of KSPE, 23*(10), 52-59.

Jhurani, S.M., & Fred Higgs, C. (2010). An elastohydrodynamic lubrication (EHL) model of wear particle migration in an artificial hip joint. *Tribology International, 43*(8), 1326-1338.

Kamaraj, Abishek B, Sundaram, Murali M, & Mathew, Ronnie. (2013). Ultra high aspect ratio penetrating metal microelectrodes for biomedical applications. *Microsystem Technologies, 19*(2), 179-186.

Katz, Z, & Tibbles, CJ. (2005). Analysis of micro-scale EDM process. *The International Journal of Advanced Manufacturing Technology, 25*(9-10), 923-928.

Khan, Zulfiqar Ahmad, & Hadfield, Mark. (2007). Manufacturing induced residual stress influence on the rolling contact fatigue life performance of lubricated silicon nitride bearing materials. *Materials & Design, 28*(10), 2688-2693. doi: http://dx.doi.org/10.1016/j.matdes.2006.10.003

Khan, Zulfiqar Ahmad, Hadfield, Mark, Tobe, Shogo, & Wang, Ying. (2005). Ceramic rolling elements with ring crack defects—A residual stress approach. *Materials Science and Engineering: A, 404*(1–2), 221-226.

Khan, Zulfiqar Ahmad, Hadfield, Mark, Tobe, Shogo, & Wang, Ying. (2006). Residual stress variations during rolling contact fatigue of refrigerant lubricated silicon nitride bearing elements. *Ceramics International, 32*(7), 751-754.

Kilickap, Erol, & Huseyinoglu, Mesut. (2010). Selection of optimum drilling parameters on burr height using response surface methodology and genetic algorithm in drilling of AISI 304 stainless steel. *Materials and Manufacturing Processes, 25*(10), 1068-1076.

Kim, Beomkeun, Chae, Young Hun, & Choi, Heung Soap. (2014). Effects of surface texturing on the frictional behavior of cast iron surfaces. *Tribology International, 70*, 128-135.

Kovalchenko, A., Ajayi, O., Erdemir, A., & Fenske, G. (2011). Friction and wear behavior of laser textured surface under lubricated initial point contact. *Wear, 271*(9), 1719-1725.

Kovalchenko, A., Ajayi, O., Erdemir, A., Fenske, G., & Etsion, I. (2005). The effect of laser surface texturing on transitions in lubrication regimes during unidirectional sliding contact. *Tribology International, 38*(3), 219-225.

Křupka, I., & Hartl, M. (2007). The effect of surface texturing on thin EHD lubrication films. *Tribology international, 40*(7), 1100-1110.

Křupka, I., & Hartl, M. (2009). Effect of Surface Texturing on Very Thin Film EHD Lubricated Contacts. *Tribology Transactions, 52*(1), 21-28.

Krupka, I., Svoboda, P., & Hartl, M. (2010). Effect of surface topography on mixed lubrication film formation during start up under rolling/sliding conditions. *Tribology International, 43*(5), 1035-1042.

Křupka, I., Vrbka, M., & Hartl, M. (2008). Effect of surface texturing on mixed lubricated non-conformal contacts. *Tribology International, 41*(11), 1063-1073.

Křupka, Ivan, & Hartl, Martin. (2008). Effect of Surface Texturing on Very Thin Film EHD Lubricated Contacts. *Tribology Transactions, 52*(1), 21-28.

Li, J., Zhou, F., & Wang, X. (2011). Modify the friction between steel ball and PDMS disk under water lubrication by surface texturing. *Meccanica, 46*(3), 499-507.

Liu, Hongbin, Niu, Rongjun, & Meng, Yonggang. (2010). The Effect of Laser Texturing of Steel Surfaces on Film Lubriction Based on Stribeck Curves *Advanced Tribology* (pp. 685-687): Springer.

Llanes, L, Idanez, E, Martínez, E, Casas, B, & Esteve, J. (2001). Influence of electrical discharge machining on the sliding contact response of cemented carbides. *International Journal of Refractory Metals and Hard Materials, 19*(1), 35-40.

Love, CA, Cook, RB, Harvey, TJ, Dearnley, PA, & Wood, RJK. (2012). Diamond like carbon coatings for potential application in biological implants–a review. *Tribology International*, 63, 141 – 150.

Lu, X., & Khonsari, MM. (2007). An experimental investigation of dimple effect on the Stribeck curve of journal bearings. *Tribology Letters, 27*(2), 169-176.

Ma, Chenbo, & Zhu, Hua. (2011). An optimum design model for textured surface with elliptical-shape dimples under hydrodynamic lubrication. *Tribology International, 44*(9), 987-995.

Masuzawa, T, Kuo, C-L, & Fujino, MIIS. (1994). A combined electrical machining process for micronozzle fabrication. *CIRP Annals-Manufacturing Technology, 43*(1), 189-192.

Masuzawa, Takahisa. (2000). State of the art of micromachining. *CIRP Annals-Manufacturing Technology, 49*(2), 473-488.

Meijer, J, Du, K, Gillner, A, Hoffmann, D, Kovalenko, VS, Masuzawa, T, . . . Schulz, W. (2002). Laser machining by short and ultrashort pulses, state of the art and new opportunities in the age of the photons. *CIRP Annals-Manufacturing Technology, 51*(2), 531-550.

Meijer, Johan. (2004). Laser beam machining (LBM), state of the art and new opportunities. *Journal of Materials Processing Technology, 149*(1–3), 2-17.

Mischler, Stefano, & Muñoz, Anna Igual. (2012). Wear of CoCrMo alloys used in metal-on-metal hip joints: A tribocorrosion appraisal. *Wear*, 297(1-2), 1081 – 1094.

Mohd Abbas, Norliana, Solomon, Darius G, & Fuad Bahari, Md. (2007). A review on current research trends in electrical discharge machining (EDM). *International Journal of Machine Tools and Manufacture, 47*(7), 1214-1228.

Mourier, L., Mazuyer, D., Lubrecht, AA, & Donnet, C. (2006). Transient increase of film thickness in micro-textured EHL contacts. *Tribology international, 39*(12), 1745-1756.

Nakano, M., Korenaga, A., Korenaga, A., Miyake, K., Murakami, T., Ando, Y., . . . Sasaki, S. (2007). Applying micro-texture to cast iron surfaces to reduce the friction coefficient under lubricated conditions. *Tribology Letters, 28*(2), 131-137.

Nine, Md J, Choudhury, Dipankar, Hee, Ay Ching, Mootanah, Rajshree, & Osman, Noor Azuan Abu. (2014). Wear Debris Characterization and Corresponding Biological Response: Artificial Hip and Knee Joints. *Materials, 7*(2), 980-1016.

PAJAK, P.T., SILVA, A.K.M. DE, HARRISON, D.K., & McGEOUGH, J.A. (2005). Resesrch and development in laser beam machining. *Budowa Maszyn i Zarazadzanie Produkcja, Nr 2*, 29.

Park, BJ, Kim, BH, & Chu, CN. (2006). The effects of tool electrode size on characteristics of micro electrochemical machining. *CIRP Annals-Manufacturing Technology, 55*(1), 197-200.

Park, Min Soo, & Chu, Chong Nam. (2007). Micro-electrochemical machining using multiple tool electrodes. *Journal of Micromechanics and Microengineering, 17*(8), 1451.

Parreira, JG, Gallo, CA, & Costa, HL. (2012). New Advances on Maskless Electrochemical Surface Texturing (MECT) for Tribological Purposes. *Surface and Coatings Technology*. *212*, 1 – 13.

Pavlinich, SP, Mannapov, AR, Gimaev, NZ, & Zaitsev, AN. (2008). Electrochemical shaping of aerodynamic seal elements. *Russian Aeronautics (Iz VUZ), 51*(3), 330-338.

Podgornik, B, Vilhena, LM, Sedlaček, M, Rek, Z, & Žun, I. (2012). Effectiveness and design of surface texturing for different lubrication regimes. *Meccanica, 47*(7), 1613-1622.

Puri, AB, & Bhattacharyya, B. (2003). Modelling and analysis of the wire-tool vibration in wire-cut EDM. *Journal of materials processing technology, 141*(3), 295-301.

Qian, S., Zhu, D., Qu, N., Li, H., & Yan, D. (2010). Generating micro-dimples array on the hard chrome-coated surface by modified through mask electrochemical micromachining. *The International Journal of Advanced Manufacturing Technology, 47*(9), 1121-1127.

Qiu, Y., & Khonsari, MM. (2011). Experimental investigation of tribological performance of laser textured stainless steel rings. *Tribology International, 44*(5), 635-644.

Rajurkar, KP, Sundaram, MM, & Malshe, AP. (2013). Review of Electrochemical and Electrodischarge Machining. *Procedia CIRP, 6*, 13-26.

Rajurkar, KP, & Wang, WM. (1993). Thermal modeling and on-line monitoring of wire-EDM. *Journal of Materials Processing Technology, 38*(1), 417-430.

Rajurkar, KP, Wang, ZY, & Kuppattan, A. (1999). Micro removal of ceramic material (Al_2O_3) in the precision ultrasonic machining. *Precision Engineering, 23*(2), 73-78.

Rajurkar, KP, & Yu, ZY. (2000). 3d micro-edm using cad/cam. *CIRP Annals-Manufacturing Technology, 49*(1), 127-130.

Rajurkar, KP, Zhu, Di, McGeough, JA, Kozak, J, & De Silva, A. (1999). New developments in electro-chemical machining. *CIRP Annals-Manufacturing Technology, 48*(2), 567-579.

Ramesh, A., Akram, W., Mishra, S.P., Cannon, A.H., Polycarpou, A.A., & King, W.P. (2012). Friction characteristics of microtextured surfaces under mixed and hydrodynamic lubrication. *Tribology International*. *57*, 170 – 176.

Roualdes, O., Duclos, M.E., Gutknecht, D., Frappart, L., Chevalier, J., & Hartmann, D.J. (2010). In vitro and in vivo evaluation of an alumina–zirconia composite for arthroplasty applications. *Biomaterials, 31*(8), 2043-2054.

Roy, Taposh, Choudhury, Dipankar, Bin Mamat, Azuddin, & Pingguan-Murphy, Belinda. (2014). Fabrication and characterization of micro-dimple array on Al2O3 surfaces by using a micro-tooling. *Ceramics International, 40*(1), 2381-2388.

Sampedro, J, Ferre, R, Fernández, E, Pérez, I, Cárcel, B, Molina, T, & Ramos, JA. (2012). Surface Functionalization of AISI 316 Steel by Laser Texturing of Shaped Microcavities with Picosecond Pulses. *Physics Procedia, 39*, 636-641.

Sawano, H., Warisawa, S., & Ishihara, S. (2009a). Study on long life of artificial joints by investigating optimal sliding surface geometry for improvement in wear resistance. *Precision Engineering-Journal of the International Societies for Precision Engineering and Nanotechnology, 33*(4), 492-498.

Sawano, H., Warisawa, S., & Ishihara, S. (2009b). Study on long life of artificial joints by investigating optimal sliding surface geometry for improvement in wear resistance. *Precision Engineering, 33*(4), 492-498.

Shin, Hong Shik, Park, Min Soo, Kim, Bo Hyun, & Chu, Chong Nam. (2011). Recent researches in micro electrical machining. *International Journal of Precision Engineering and Manufacturing, 12*(2), 371-380.

Singh, Rupinder, & Khamba, JS. (2006). Ultrasonic machining of titanium and its alloys: a review. *Journal of materials processing technology, 173*(2), 125-135.

Singh, Shankar, Maheshwari, S, & Pandey, PC. (2004). Some investigations into the electric discharge machining of hardened tool steel using different electrode materials. *Journal of Materials Processing Technology, 149*(1), 272-277.

Spur, Günter, & Holl, S-E. (1996). Ultrasonic assisted grinding of ceramics. *Journal of Materials Processing Technology, 62*(4), 287-293.

Suh, M. S., Chae, Y. H., Kim, S. S., Hinoki, T., & Kohyama, A. (2010). Effect of geometrical parameters in micro-grooved crosshatch pattern under lubricated sliding friction. *Tribology International, 43*(8), 1508-1517.

Takami, Yoshiyuki, Nakazawa, Tadashi, Makinouchi, Kenzo, Glueck, Julie, & Nosé, Yukihiko. (1997). Biocompatibility of alumina ceramic and polyethylene as materials for pivot bearings of a centrifugal blood pump. *Journal of biomedical materials research, 36*(3), 381-386.

Taniguchi, Norio. (1983). Current status in, and future trends of, ultraprecision machining and ultrafine materials processing. *CIRP Annals-Manufacturing Technology, 32*(2), 573-582.

Tawakoli, Taghi, Azarhoushang, Bahman, & Rabiey, Mohammad. (2009). Ultrasonic assisted dry grinding of 42CrMo4. *The International Journal of Advanced Manufacturing Technology, 42*(9-10), 883-891.

Tay, NamBeng, Minn, Myo, & Sinha, SujeetK. (2011). A Tribological Study of SU-8 Micro-Dot Patterns Printed on Si Surface in a Flat-on-Flat Reciprocating Sliding Test. *Tribology Letters, 44*(2), 167-176.

Thoe, TB, Aspinwall, DK, & Killey, N. (1999). Combined ultrasonic and electrical discharge machining of ceramic coated nickel alloy. *Journal of Materials Processing Technology, 92*, 323-328.

Uehara, Y., Wakuda, M., Yamauchi, Y., Kanzaki, S., & Sakaguchi, S. (2004). Tribological properties of dimpled silicon nitride under oil lubrication. *Journal of the European Ceramic Society, 24*(2), 369-373.

Vilhena, L. M., Sedlaček, M., Podgornik, B., Vižintin, J., Babnik, A., & Možina, J. (2009). Surface texturing by pulsed Nd:YAG laser. *Tribology International, 42*(10), 1496-1504.

Wakuda, M., Yamauchi, Y., Kanzaki, S., & Yasuda, Y. (2003). Effect of surface texturing on friction reduction between ceramic and steel materials under lubricated sliding contact. *Wear, 254*(3), 356-363.

Wang, Chicheng J., Hong, Min S., & Ehmann, Kornel F. (1994). Surface Topography Control in Single-Point Cutting. *S.M. Wu Symposium*.

Wang, X., Adachi, K., Otsuka, K., & Kato, K. (2006). Optimization of the surface texture for silicon carbide sliding in water. *Applied Surface Science, 253*(3), 1282-1286.

Wang, X., Kato, K., Adachi, K., & Aizawa, K. (2001). The effect of laser texturing of SiC surface on the critical load for the transition of water lubrication mode from hydrodynamic to mixed. *Tribology International, 34*(10), 703-711.

Wang, X., Kato, K., Adachi, K., & Aizawa, K. (2003). Loads carrying capacity map for the surface texture design of SiC thrust bearing sliding in water. *Tribology International, 36*(3), 189-197.

Wang, X., Liu, W., Zhou, F., & Zhu, D. (2009). Preliminary investigation of the effect of dimple size on friction in line contacts. *Tribology International, 42*(7), 1118-1123.

Wansheng, Zhao, Zhenlong, Wang, Shichun, Di, Guanxin, Chi, & Hongyu, Wei. (2002). Ultrasonic and electric discharge machining to deep and small hole on titanium alloy. *Journal of Materials Processing Technology, 120*(1), 101-106.

Widmer, Martin R, Heuberger, Manfred, Vörös, Janos, & Spencer, Nicholas D. (2001). Influence of polymer surface chemistry on frictional properties under protein-lubrication conditions: implications for hip-implant design. *Tribology Letters, 10*(1-2), 111-116.

Yamakiri, Hiroki, Sasaki, Shinya, Kurita, Tsuneo, & Kasashima, Nagayoshi. (2011). Effects of laser surface texturing on friction behavior of silicon nitride under lubrication with water. *Tribology International, 44*(5), 579-584.

Yan, BH, Wang, AC, Huang, CY, & Huang, FY. (2002). Study of precision micro-holes in borosilicate glass using micro EDM combined with micro ultrasonic vibration machining. *International journal of machine tools and manufacture, 42*(10), 1105-1112.

Yan, Dongsheng, Qu, Ningsong, Li, Hansong, & Wang, Xiaolei. (2010). Significance of dimple parameters on the friction of sliding surfaces investigated by orthogonal experiments. *Tribology Transactions, 53*(5), 703-712.

Yang, Insoon, Park, Min Soo, & Chu, Chong Nam. (2009). Micro ECM with ultrasonic vibrations using a semi-cylindrical tool. *International Journal of Precision Engineering and Manufacturing, 10*(2), 5-10.

Yanyan, Yan, Bo, Zhao, & Junli, Liu. (2009). Ultraprecision surface finishing of nano-ZrO2 ceramics using two-dimensional ultrasonic assisted grinding. *The International Journal of Advanced Manufacturing Technology, 43*(5-6), 462-467.

Yeo, SH, & Tan, LK. (1999). Effects of ultrasonic vibrations in micro electro-discharge machining of microholes. *Journal of micromechanics and microengineering, 9*(4), 345.

Yu, Haiwu, Wang, Xiaolei, & Zhou, Fei. (2010). Geometric Shape Effects of Surface Texture on the Generation of Hydrodynamic Pressure Between Conformal Contacting Surfaces. *Tribology Letters, 37*(2), 123-130. doi: 10.1007/s11249-009-9497-4

Yu, ZY, Masuzawa, T, & Fujino, M. (1998). Micro-EDM for three-dimensional cavities-development of uniform wear method. *CIRP Annals-Manufacturing Technology, 47*(1), 169-172.

Yuan, Sihuan, Huang, Wei, & Wang, Xiaolei. (2011). Orientation effects of micro-grooves on sliding surfaces. *Tribology International, 44*(9), 1047-1054.

Zhixin, Jia, Jianhua, Zhang, & Xing, Ai. (1995). Ultrasonic vibration pulse electro-discharge machining of holes in engineering ceramics. *Journal of materials processing technology, 53*(3), 811-816.

Zhou, Rui, Cao, Jian, Wang, Q Jane, Meng, Fanming, Zimowski, Krystian, & Xia, Z Cedric. (2011). Effect of EDT surface texturing on tribological behavior of aluminum sheet. *Journal of Materials Processing Technology, 211*(10), 1643-1649.

Zhou, Xincong, Galvin, Alison L, Jin, Zhongmin, Yan, Xinping, & Fisher, J. (2012). The influence of concave dimples on the metallic counterface on the wear of ultra-high molecular weight polyethylene. *Proceedings of the Institution of Mechanical Engineers, Part J: Journal of Engineering Tribology, 226*(6), 455-462.

Zhu, DNSQ, Qu, NS, Li, HS, Zeng, YB, Li, DL, & Qian, SQ. (2009). Electrochemical micromachining of microstructures of micro hole and dimple array. *CIRP Annals-Manufacturing Technology, 58*(1), 177-180.

PUBLICATIONS

Taposh Roy, Dipankar Choudhury, Azuddin Bin Mamat and Belinda Pingguan-Murphy, Fabrication and characterization of micro dimple array on Al_2O_3 surfaces by using a micro-tooling; Ceramic International, Volume 40, Issue 1, Part B, January 2014, Pages 2381–2388.

Dipankar Choudhury, Robert Walker, **Taposh Roy,** Sweety Paul and Rajshree Mootanah, Performance of honed Surface profiles to Artificial Hip Joints: An Experimental Investigation; International Journal of Precision Engineering and Manufacturing, Volume 14, Issue10, October 2013, Pages. 1847-1853.

Dipankar Choudhury, **Taposh Roy**, Ivan Krupka, Martin Hartl, Rajshree Mootanah; Tribological properties of ultra-high molecular weight polyethylene against advanced ceramic surfaces in total hip joint replacement, Proceedings of the Institution of Mechanical Engineers, Part J: Journal of Engineering Tribology (Online)

Taposh Roy, Dipankar Choudhury, Belinda Pingguan-Murphy; The effect of micro tools fabricated dent on alumina/alumina oxide interface, World Academy of Science, Engineering and Technology International Journal of Medical, Pharmaceutical Science and Engineering, Volume 7, Issue 11, November 2013.

Taposh Roy, Dipankar Choudhury, Subir Ghosh, Azuddin Bin B Mamat, Belinda Pingguan- P Murphy; Improved friction and wear performance of micro dimple ceramic-on-ceramic interface for hip joint arthroplasty, Ceramic International(Under review).

APPENDIX A-

Residual stress calculation by XRD analysis

To determine the surface profile and to select a suitable peak for residual stress measurement, Samples with dimples were scanned in 2θ region from 30 to 150 as shown in Figure A-1. As a criterion to determine the residual stress using the XRD-$\sin^2\psi$ technique, the selection of diffraction peak should have the following characteristics.

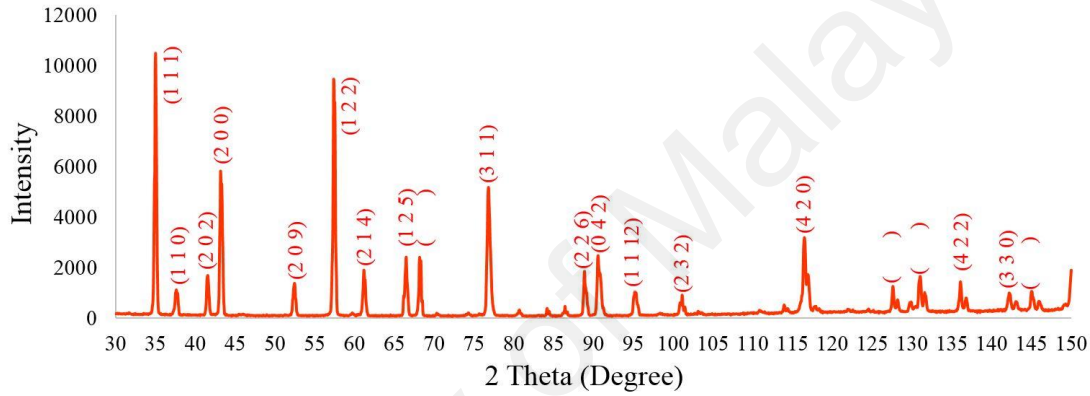

Figure A-1: X-ray diffraction peaks of samples

1. The diffraction peak should be higher in Bragg angle (2θ). Typically residual stress is measured by the Bragg angles that occur at more than 130º. In this experiment, the intensities of the peaks were very insignificant when 2θ>120º. For this reason, peaks that occurred below 120º in 2θ angle were considered to calculate the residual stress.

2. The selected diffraction peak should not overlap with other diffraction peaks. For this reason, peaks in this region where peaks that occur at approximately 115º and 118º were selected for residual stress analysis.

3. The diffraction peak should be single and well-shaped with high intensity. The peak from the (420) crystal planes of the sample that occurred at approximately 116º

possessed all the properties required to determine the residual stress. This peak was selected to investigate further for residual stress measurements.

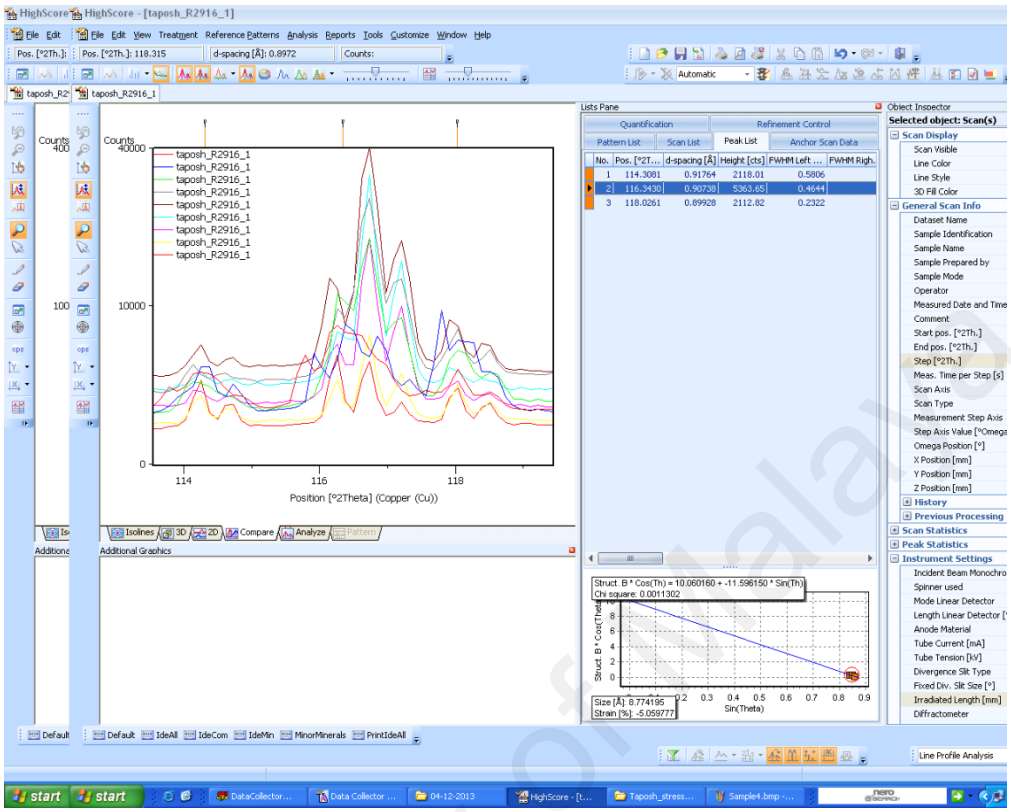

Figure A-2: Slow scan of the sample crystal peak (420) of total 9 scans

Samples were further scanned in the 2θ region from 113.5º to 119.5º at different tilt angles (ψ) with a slow scanning speed. The tilt angles were varied from -40ºto 40ºas shown in Figure A-2. The lattice spacing (d) was plotted against $\sin^2 \psi$ as shown in Figure A-3.

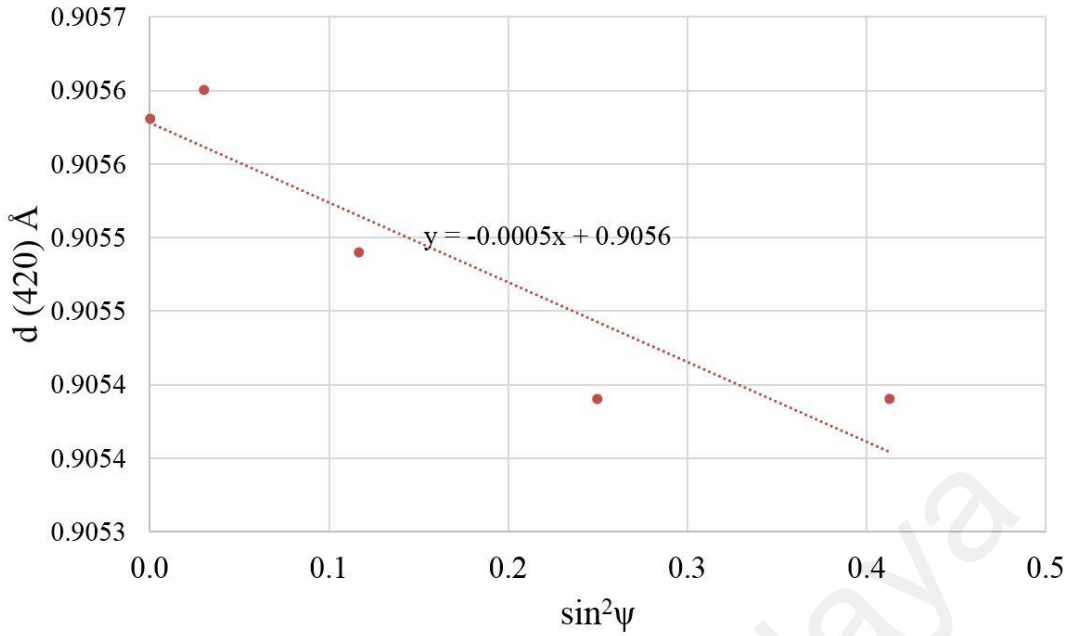

Figure A-3: d- $\sin^2 \psi$ plot of the crystal peak (420) of the sample

The residual stress of the particles was calculated by the following formula

$$\sigma = \frac{E}{1+\vartheta} * \alpha$$

Where σ is the residual stress,

Young's modulus, E =375 GPa,

Poison ratio, ϑ = 0.22

And slope of the 2θ–$\sin^2 \psi$ curve, α= -0.0005.

Now,

$$\sigma = \frac{375*1E9}{(1+0.22)} * (-0.0005)$$

= -153.6 Mpa